GeoScience Engineering

INTEGRATION OF MAGNETIC RESIDUALS, DERIVATIVES AND LOCATED EULER DECONVOLUTION FOR STRUCTURAL AND GEOLOGIC MAPPING OF PARTS OF THE PRECAMBRIAN GNEISSES OF AGO-IWOYE, SOUTHWESTERN NIGERIA

Stephen O. ARIYO[1], Joseph O. COKER[2], Afolabi O. ALAKA [1], Omolara A. ADENUGA[2], Olateju O. BAYEWU[1]

[1] *Department of Earth Sciences, Olabisi Onabanjo University, Ago-Iwoye, Ogun State*

[2]*Department of Physics, Olabisi Onabanjo University, Ago-Iwoye, Ogun State*

Email: stephen.o.ariyo@oouagoiwoye.edu.ng

ABSTRACT

Ground based magnetic survey conducted between longitude 06O 55I 51IIN – 06O 55I 54IIN and latitude 03O 52I 06IIE – 03O 52I 4.8IIE (Olabisi Onabanjo University) remarkably revealed a consistent subsurface NW - SE structural azimuth of localized discontinuities within the shallowly buried heterogeneous basement rocks, which at exposed locations are composed of strongly foliated granite gneiss and migmatite-gneiss with veins and veinlets principally orientated in NNW – SSE direction. Magnetic survey of the area was preceded by site inspection to avoid metallic objects interferences. Field procedure in the area involved Cartesian gridding, base station establishment, data acquisition at gridded points, and repeated bihourly diurnal checks at the base station. At the processing stage, diurnal variation effect was aptly removed before subjection to Kriging (gridding). The gridded data was then prepared as input for Forward Fourier Filter Transform (FFT), which upon definition and implementation enabled Butterworth filtering of isolated ringing effects, reduction to the equator (RTE) for geomagnetic correction, and the use of Gaussian and Upward Continuation filtering for regional magnetic intensity trend determination. Removal of the regional magnetic intensity (RMI) from the total magnetic intensity (TMI) resulted in the derivation of the residual anomaly. Enhancement filters adopted for better resolution of the residual magnetic gradient include analytical signal (AS), tilt-angle derivative (TDR), vertical derivative deconvolution (VDD), and the first vertical derivatives (FVD). TMI and RMI values range between 32925nT – 33050nT and 32935nT – 333050nT respectively, while the residual gradient ranges between 15nT/m and 10nT/m; AS ranges between 0.28nT/m and 4.1nT/m; and TDR ranges from -1.4nT/m to 1.4nT/m. Source depth calculation estimated from power spectrum analysis and Euler deconvolution ranges between 1m and 15m. Composite overlay of magnetic maps revealed jointed and faulted zones within the area; exhibiting a NW-SE principal azimuth of Liberian orogenic impress, which are in consistence with the foliation direction of the jagged foliated bedrock with an estimated maximum overburden of about 15m. The structural significance of this area as a prospective hydro-geological centre, and as an undesirable spot for high-rise building has been accurately evaluated from research findings. Application of integrated geophysical approach, complemented by detailed geological studies may furnish greater information about the subsurface structural architecture.

Keywords: Gneisses; Ground Magnetic Surveying; RTE; Structural discontinuities; TDR.

1 INTRODUCTION

Structural mapping is an integral part of geologic surveys. It involves measurements, analyses, interpretation and recognition of geometrical features (structures) generated by rock deformations [1]. These structures often serve as fountains of environmental challenges or unparalleled opportunities depending on their modes of occurrences, which in most cases are imminently controlled by the dynamic interplay of differential stress distributions within the earth interior. In line with the principle of uniformitarianism, a broad understanding about Earth's paleo processes and internal workings are deductible from the various deformation types for diverse applications. Deductible inferences from brittle deformations include the kinematics of crustal blocks, orientation of principal axes of regional and local stresses, and geometry. Deeper insights in deep seated stresses, regional movements and block motions are obtainable from ductile deformations.

Volume 66 (2020), No. 1
p. 1 – 32, ISSN 1802-5420
DOI 10.35180/gse-2020-0027

Basement structures are essentially significant for several well-known exploration and environmental motives. Structural fabric of basement rocks when interpreted may deduce the deformative patterns and the magnitude of causative stress impact responsible for deformation. The genetic occurrences of most mineralizations and groundwater accumulations in basement terrain are structurally controlled [2]; hence, requiring the need for the detection and identification of the critical geological structures. Structural indicators used for tracking geological anomalies include fractures, non-conformities, folds, and shear zones. Consideration of spatial imminence to these structures during prospecting increases the chances of exploration success [3] as localization of many mineralization anomalies extends profoundly into the surrounding hosts.

Prolific spots commonly targeted during exploration include lineament junctions, intersection of composite structures (e.g. fractured fold, sheared faulted or folded zone). Lineament intersection patterns on structural maps occur in various forms, notably as 'X', 'Y' and 'Z' crosses; other intersection styles are also possible depending on the principal axes of the exerted stresses on the rock body.

The significance of a lineament differs markedly across different geologic provinces due to the diversity in petrological characters. A fracture system crosscutting a non-mineralized basement is most likely to function as secondary groundwater conduit if other hydrogeological indices (recharge rate, transmissivity, storativity and regolith structure) are favourable. Around an igneous emplacement or metamorphic aureole, linear discontinuities (lineaments) aid as facilitating conduit for ion-rich hydrothermal fluid circulation and groundwater remobilization which upon cooling may precipitate minerals (ores) of economic interests within the structure.

Magnetic method of lineament extractions essentially involves the interpretation of susceptibility anomalies along linear magnetic lows, linear magnetic highs, elongated zones of high magnetic gradients, and magnetic offsets of similarly dislocated units; all of which are brought about by the internal structural dynamics of the earth interior. Anomalous linear magnetic 'lows' are characteristics of demagnetized silica vein, fractured zone, shear zone or other rock weaknesses compounded by weathering, while linear magnetic 'highs' anomalies are exhibited by choked fractures (lode deposits) infilled with ferromagnesian minerals and associated non-magnetic ores, or folded basement ridges. High amplitude, high gradient magnetic anomalies are symptomatic of bedrock depressions or dip slip displacements of basement blocks, while the offset of identical magnetic units are clearly indicative of strike slip (transform) movement of rock units. Apart from the linear anomaly types, non-linear magnetic anomalies are also commonly encountered as positive magnetic closures induced by mafic intrusion within an otherwise felsic country rock or isolated igneous intrusions within a sedimentary basin, or as negative closures induced by hydrothermally demagnetized region or quartzite (or quartz) body.

A distinctive clarification between airborne and ground magnetic surveys for the mapping of regional mega tectonic structures and localized geologic structures respectively must be noted, and for this reason, the use of the word 'lineament' in ground survey must be exclusively avoided; but for the ease of use, the term 'microlin' is introduced to define any micro-linear geologic structure with an aspect (length/width) ratio ≥20 but ≤100. Any structure below the minimum threshold is more likely to be induced from a point source. Summarily, the entire characteristics of an anomaly (amplitude, wavelength, shape and texture) within a magnetic signature must be holistically examined to narrow down the likely causative source [4]. Measurement of differential response of the studied Precambrian gneisses facies to magnetism is aimed at locating the shallow magnetic anomalies associated with structural deformations within the basement.

2 LOCATION AND ACCESSIBILITY

The magnetic grid coordinates of the first location (location A) extend from latitude 6.930268ON – 6.93125ON (Figure 1) and longitude 3.86709OE – 868502OE while the second survey centre (location B) is situated between latitude 6.933217ON – 6.93419ON and longitude 3.868154OE – 3.869491OE with a displacement of 200m NE from the location 'A'. For reconnaissance geological and accessibility studies, the geographical coverage of the area was extended to a latitude and longitude range of 6.930039ON – 6.937648ON and longitude 3.864462OE – 3.871361OE respectively. Both centres are adjacently bounded by a partly tarred minor road (University Road 2) which stretches through the university hostel to link the Ago –Ilisan Expressway in an unevenly perpendicular orientation. The area is easily accessible via a network of footpaths created within the university premises.

3 PHYSIOGRAPHIC SETTINGS

Maximum and minimum elevation recorded in the area is 46 m and 52 m respectively, inferring a maximum relief of 6 m. The topographic unevenness of this warping jagged terrain is well depicted in Figure 2; and on the basis of the contrasting elevation gradient observed in the area, the area can be classified as a low relief area characterized by two distinct zones, which are the elevated western high and the depressed contorted eastern half.

Volume 66 (2020), No. 1
p. 1–32, ISSN 1802-5420
DOI 10.35180/gse-2020-0027

Although there is no drainage channel crosscut through the area, the river system of its surrounding vicinity is largely dendritic.

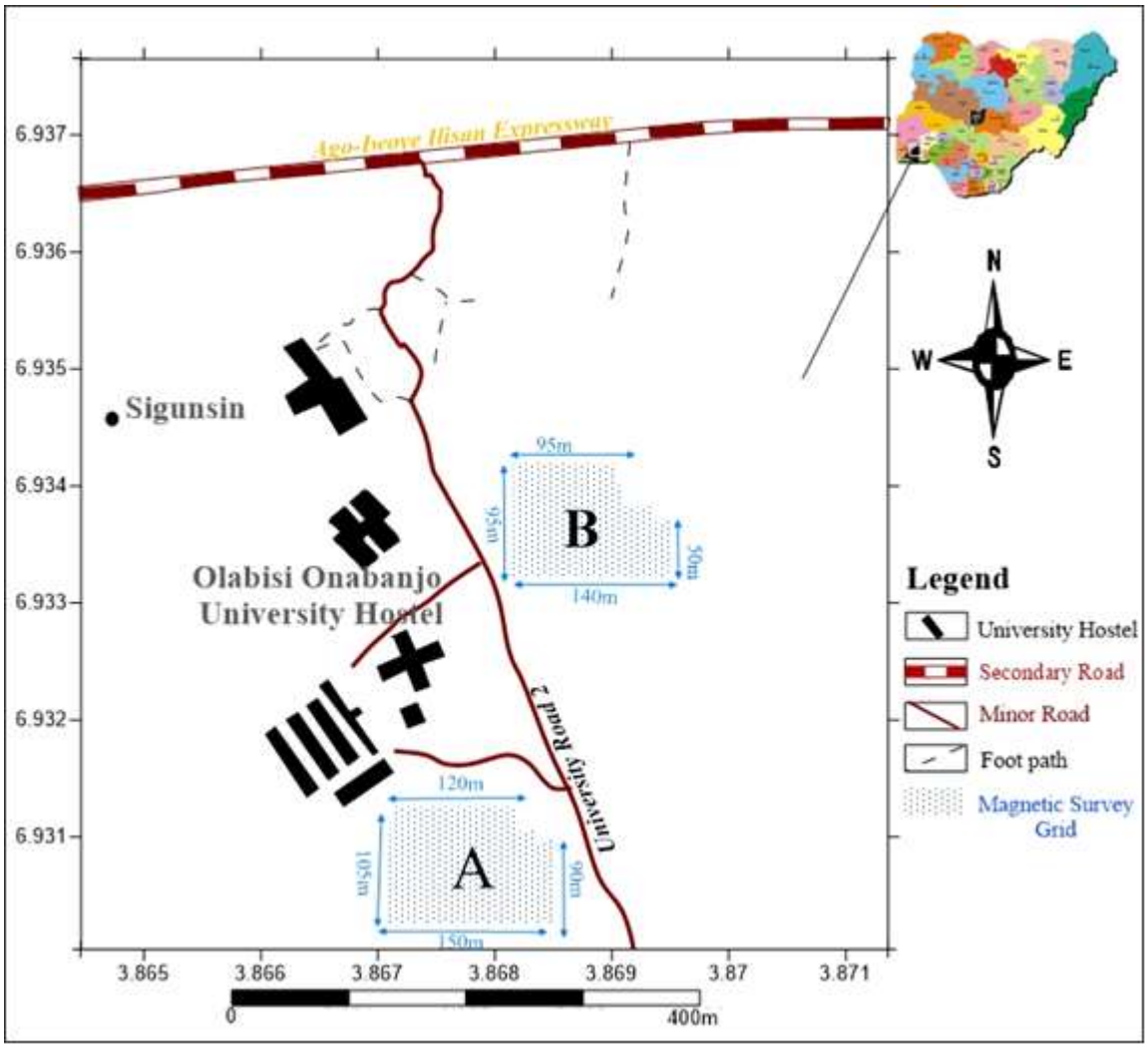

Figure 1. Location Map of the Area. 'A' and 'B' indicates the location of the first and second magnetics on the topographic map

Volume 66 (2020), No. 1
p. 1–32, ISSN 1802-5420
DOI 10.35180/gse-2020-0027

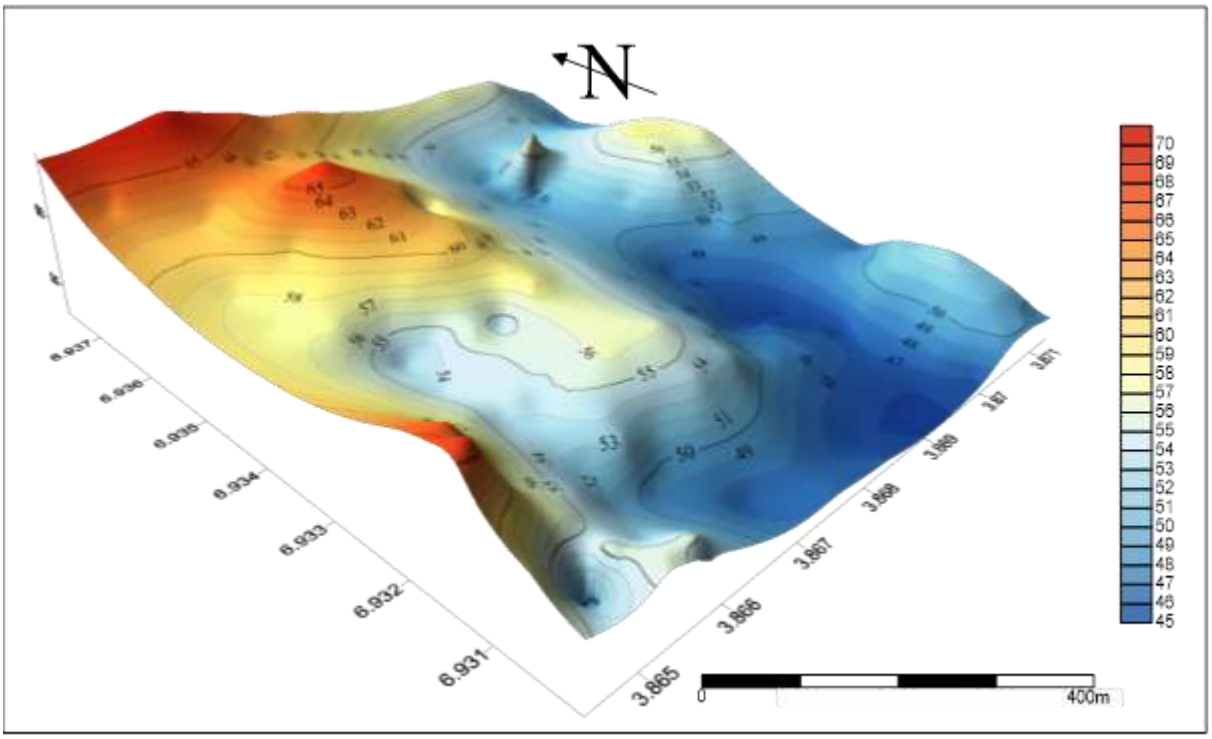

Figure 2. Topographic Map of the Study Area. Drastic drop in elevation is perceivable around the central and southern axis of the map. This relief setting could be a landscape indicator of faulting

4 GEOLOGY

Orogenic development of the Pan-African mobile belt has been widely ascribed to the crustal convergence of West African and the active Pharusian continental margin [5, 6]. Nigerian basement complex, as an integral segment of this belt, exemplifies a reactivated zone reworked by at least four classifiable orogenic phases of different chronology and deformative impresses. These orogenies provide a basis for the comprehension of the observed complexity and heterogeneity of the Nigerian crystalline terrain. Large scale regional compressions were recorded in rocks of the Liberian, Eburnean and Kibaran ages – accompanied by metamorphism and migmatization. The regional prevalence of the orogeny continued during the Pan African but was later co-ended by the development of brittle deformational structures [7, 8] through which granitic intrusive were extensively emplaced [9]. In the Jurassic, the high temperature and pressure regime stimulated the partial melting (anatexis) of the thermally less resistant felsic bands of the northern basement region; a non-orogenic process that resulted in the generation of felsic melts, and magmatic emplacement of the younger granite intrusives. Partial evacuation of the subsidiary magma chambers triggered their instability and eventual cyclic-like cauldrons within the alkaline ring complexes.

Along the Nigerian sector, the basement stretch is geometrically broken into series of discontinuous masses; exhibiting a pseudo-circular outline in the north central region, roughly triangular shape in the south western part, and as discrete pseudo-rectangular blocks in the east. Massive rock fragmentation within this belt may not be unconnected to the combined predominance of both chemical and physical weathering along the existing structural weaknesses.

Recognized lithopetrological components of the basement, in chronological order, are migmatite gneiss quartzite complex, schist belts, Pan African grainitoids, and the undeformed acid and basic dykes. Ago-Iwoye is a migmatite-gneiss terrain made up of heterogeneous migmatite, banded gneisses, granite gneisses and weakly foliated granite. Two species of gneisses occurring within the studied locality are granite gneiss and migmatite gneiss (Figure 3).

Volume 66 (2020), No. 1
p. 1–32, ISSN 1802-5420
DOI 10.35180/gse-2020-0027

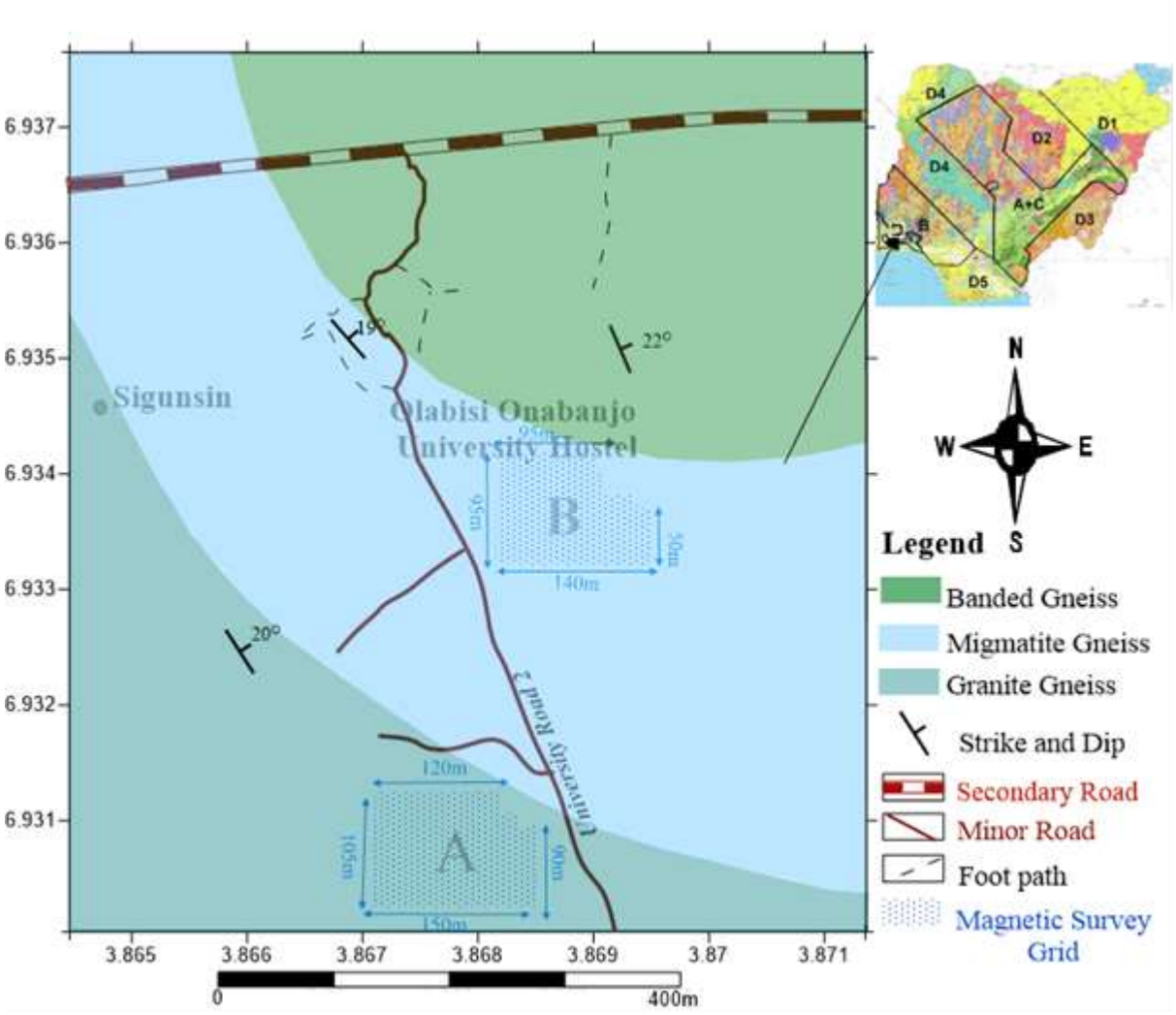

Figure 3. Geologic Map of the Study Area. Three facies of gneisses were encountered during the geologic mapping of the area, which are granite-gneiss, migmatite gneiss and granite gneiss. Grid A is situated on the granite gneiss unit, while the Grid B partly lies on an uplifted migmatite-gneiss complex. Rock exposures are generally low lying but well pronounced in the northern part. Dip of lineations is approximately 20^{O}.

5 METHODOLOGY

Advanced GSM-19T proton-precession scalar magnetometer was used for the acquisition of spatial variation in the total magnetic intensity of the study area using the gridding method of the data acquisition. Grid dimension at location 'A' is 150 m along the X (longitudinal) axis but varies between 90 m to 110 m on the Y (latitude) direction depending on the space availability along the surveyed grid line (Figure 4). At location 'B', a 140 m dimension was surveyed along the longitudinal axis but with a varying length ranging between 50 m and 100 m for the same aforementioned reason (Figure 5).

An initial round of reconnaissance inspection was embarked upon to get rid of cultural sources of magnetic interference, and to design an effective survey plan for the study area. Magnetic survey commenced over the gridded study location with the selection of a suitable spot as base station at which the first twin magnetic measurement was taken. Station interval is 5 m. The survey advances northward to the next station on the uniformly spaced Cartesian grid for the second twin measurement. The procedure was systematically repeated northward along the first longitudinal line, and then southerly down the second line (Figures 4 and 5) in that converse manner until the entire readings at the remaining stations were acquired. Diurnal fluctuation effect imposed on total magnetic intensity measurements was periodically monitored almost every two hours at the base station. The last Total Magnetic Intensity (TMI) for each day was essentially taken at the base station.

Volume 66 (2020), No. 1
p. 1–32, ISSN 1802-5420
DOI 10.35180/gse-2020-0027

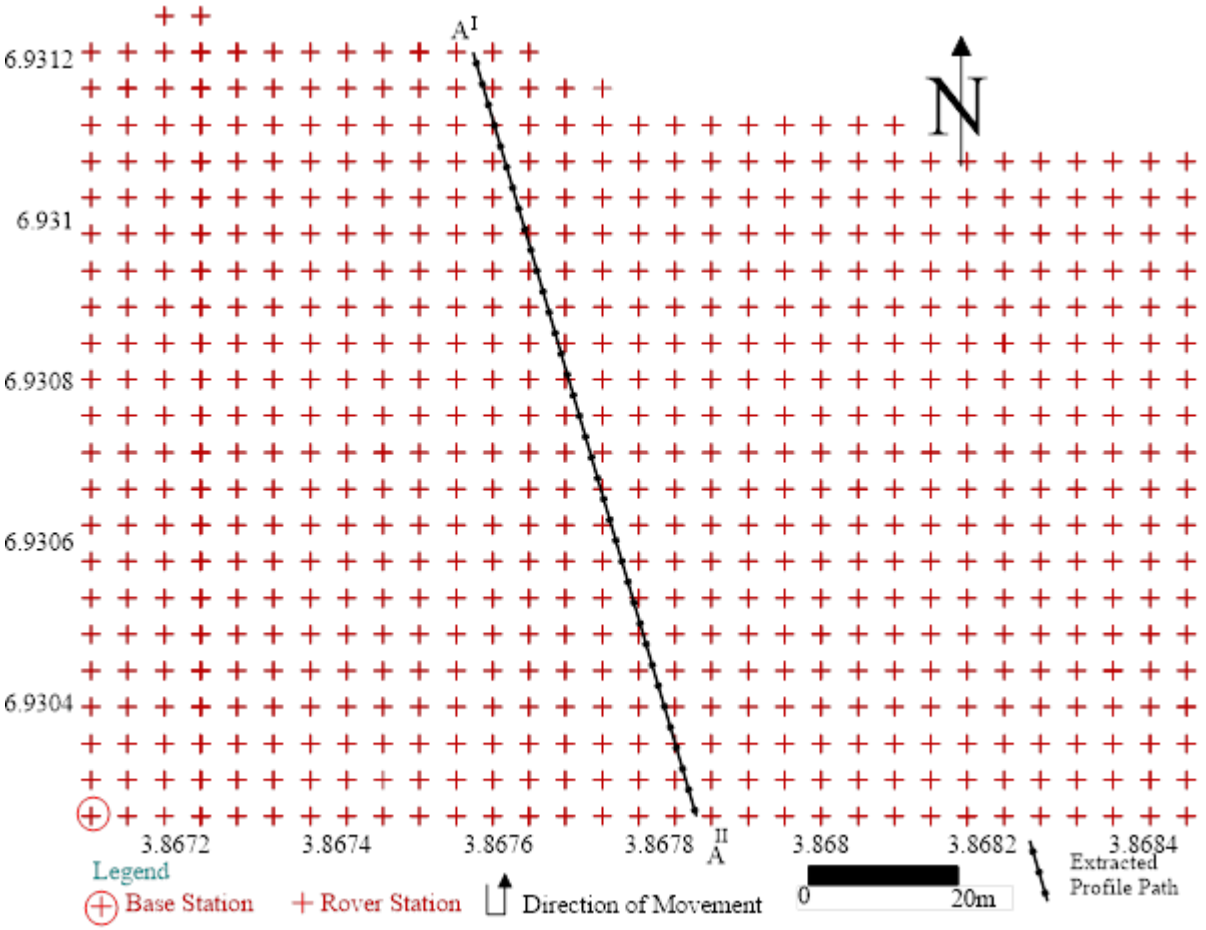

Figure 4. Survey Path Extract of Location A. Magnetic grid consists of one base station (crossed circle) at south-western corner and 641 rover stations (cross sign) spaced at a uniform interval of 5 m from one another. Profile A^{I} - A^{II} is preferentially extracted in a NNW-SSE direction to capture the most striking magnetic anomalies of interest

Volume 66 (2020), No. 1
p. 1–32, ISSN 1802-5420
DOI 10.35180/gse-2020-0027

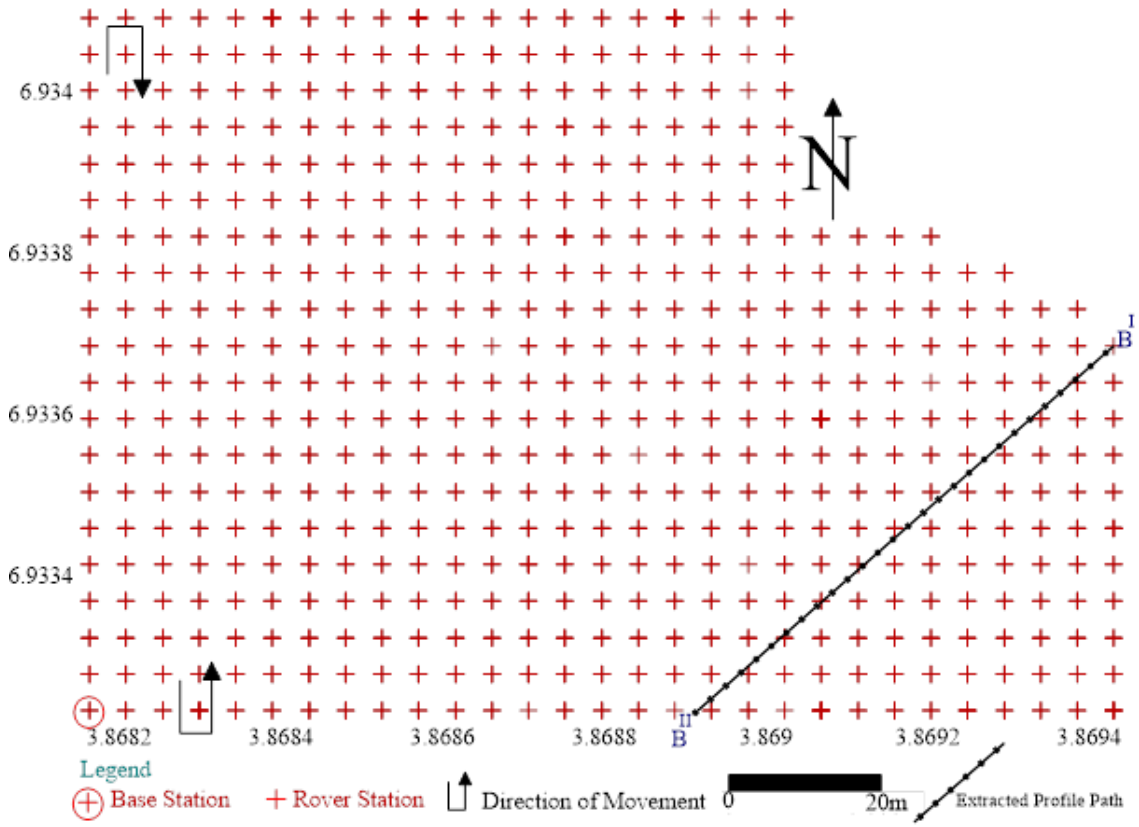

Figure 5. Survey Path Extract of Location B. Magnetic grid also consists of a base station (crossed circle) and 517 rover stations (cross sign) situated at a uniform spacing of 5 m from one another. Profile B^{I} - B^{II} extraction runs across the eastern magnetics anomalies from east to south

At the processing stage, external magnetic influences from the ionosphere and those emanating from the imperfect sphericity of the Earth were adequately removed from the field data in order to detect the anomaly pattern of the investigated subsurface. Magnitude of diurnal variation on the graphical plot of *base station TMI* against *magnetometer time*, as observed in the area, peaked in the afternoon with increase in solar intensity but dropped to a minimum in the evening. Negative variation trend in magnetic intensity necessitated the addition of this difference from the acquired readings within the affected magnetometer time range but vice-versa for positive trend. Maximum diurnal variation on the day of acquisition ranges between 8nT and 28nT. Geomagnetic correction was enforced on the acquired data using the appropriate inclination and declination parameters calculated using the World Magnetic Model (WMM).

Sequel to the magnetic correction, the corrected Total Magnetic Intensity (TMI) data were sequentially subjected to filtering to remove the effect of ringing, and to extract both the regional and residual anomalies using the appropriate inclination and declination parameters. Furthermore, enhancement of residual magnetic gradient patterns of the area improved subsurface clarity and additionally unravelled weak subtle anomalies within the investigated basement terrain using a suite of filters. Magnetic filters employed include Butterworth, Gaussian, Upward continuation, reduction to the equator (RTE), analytical signal and tilt-angle derivative. These techniques were advantageously combined to affirm the presence of mapped anomalies.

The resulting anomaly revealed in the area was interpreted qualitatively and quantitatively. For qualitative interpretation, the direct (Kriging) contouring method was adopted for the production of magnetic maps from which structural inferences were drawn. Calculation of depth to the magnetic sources was achieved via quantitative means using automated spectral analytical technique and Euler 3-D deconvolution methods. Figure 6 below summarizes the work flow of the survey.

Volume 66 (2020), No. 1
p. 1–32, ISSN 1802-5420
DOI 10.35180/gse-2020-0027

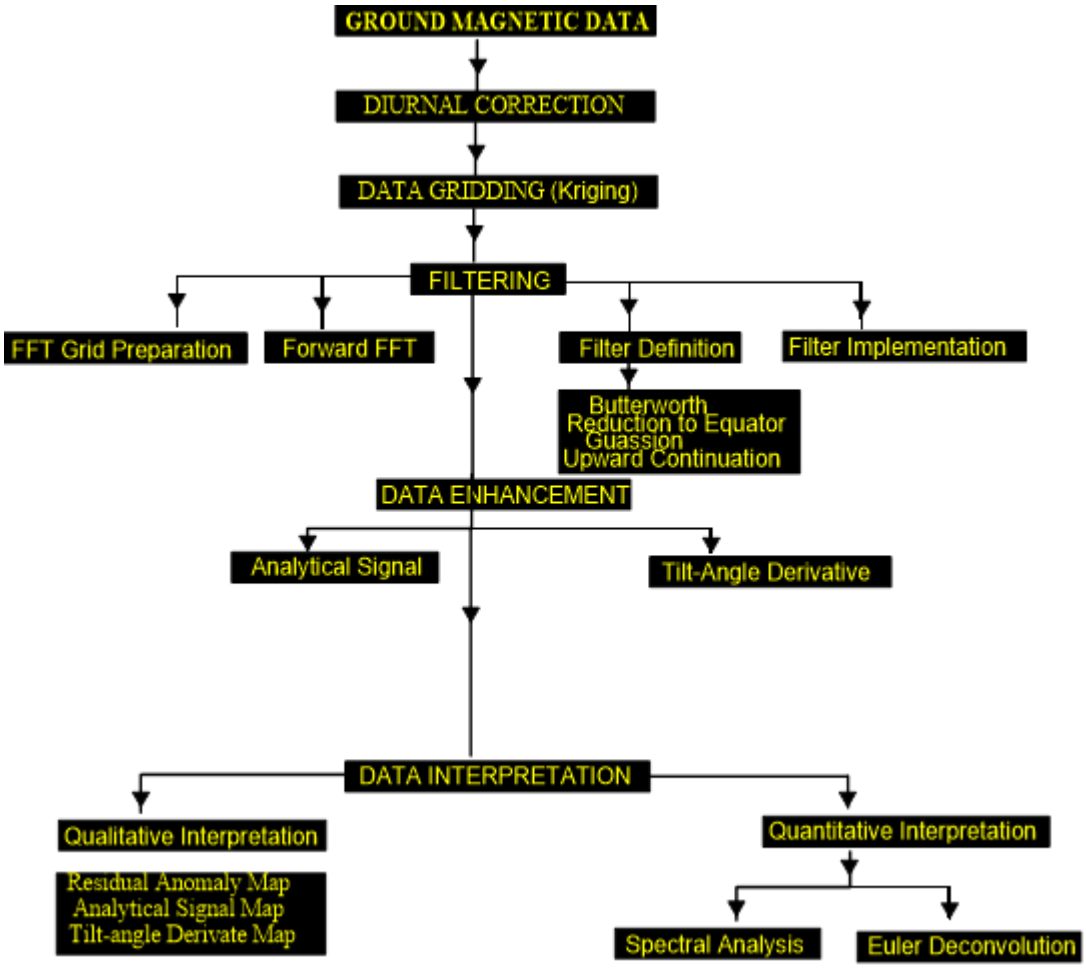

Figure 6. Flow chart algorithm

6 RESULTS

Total Magnetic Intensity (TMI) of location A and B ranged between 32950nT - 33051nT and 32920nT - 32970nT respectively (Figures 7 and 8). Upward continuation of the deep seated magnetic sources projects a decreasing west – east trend in regional magnetic intensity (RMI) at Location A, and a decreasing northwest – southeast trend at location B; corresponding RMI range is 32955nT – 33050nT and 32936nT – 32968nT (Figures 9 and 10). The resulting residual anomalies, generated upon the subtraction of the RMI from TMI grid ranges between -16nT to 34nT at the location A, and -28nT to 22nT at location B. Analytical signal range of the first and second grid ranges between 0nT –21nT and 0nT – 10nT, while the tilt angle derivative range at both locations is -1.4nT – 1.5nT. Source depth calculation estimated from power spectrum analysis and Euler deconvolution ranges between 1m – 22m.

High magnetic intensity areas are depicted on the generated magnetic maps using violet, while areas observed to be inherently characterized by low magnetic intensity are shaded blue; intermediate or quiet areas of magnetic activities are encoded with transitory colours ranging from green to yellow to red colours.

Volume 66 (2020), No. 1
p. 1–32, ISSN 1802-5420
DOI 10.35180/gse-2020-0027

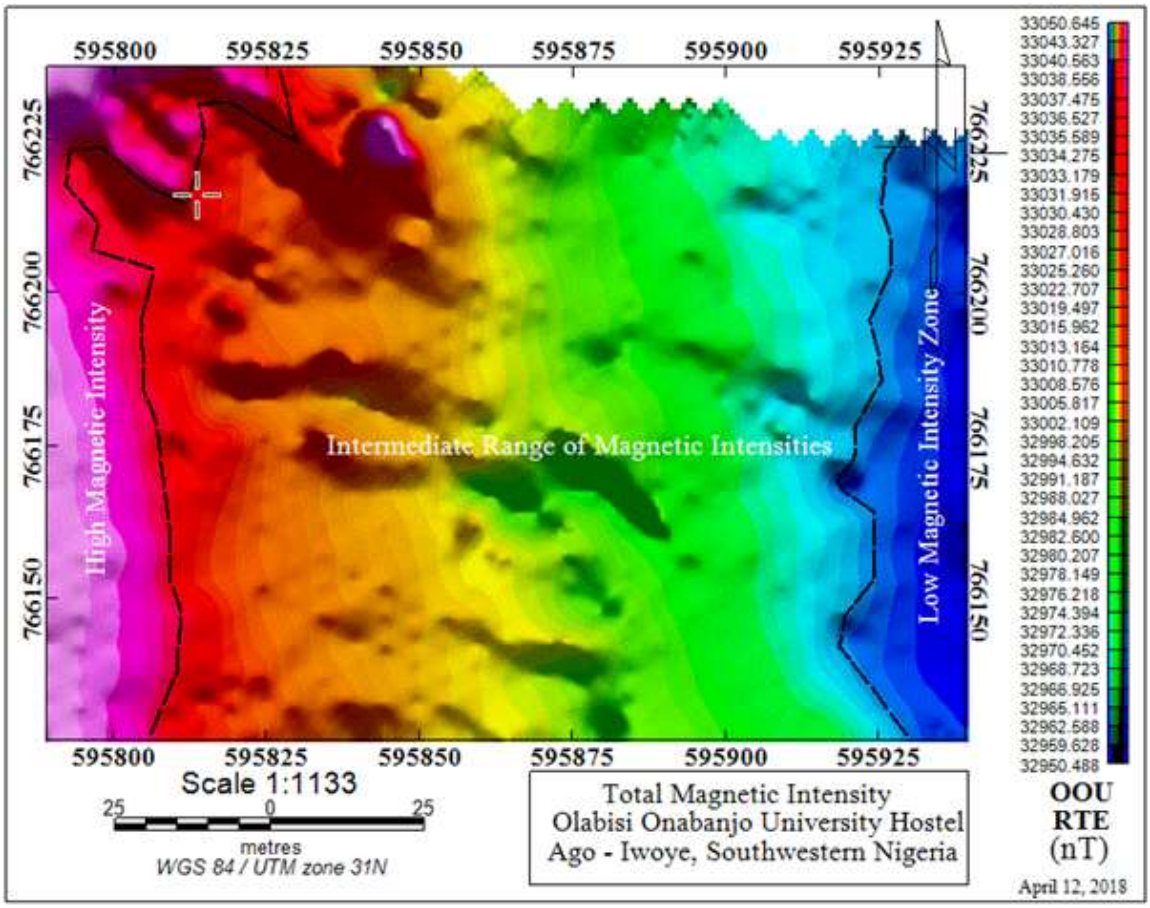

Figure 7. Total Magnetic Intensity Map of Location A. Total magnetic intensity reveals the resultant susceptibility response contributed by both near and deeply seated magnetic (geologic) bodies. Magnetic intensity is greatest (violet) along the western boundary but decreases eastward to the eastern margin, where the weakest intensities (blue) were recorded

Volume 66 (2020), No. 1
p. 1–32, ISSN 1802-5420
DOI 10.35180/gse-2020-0027

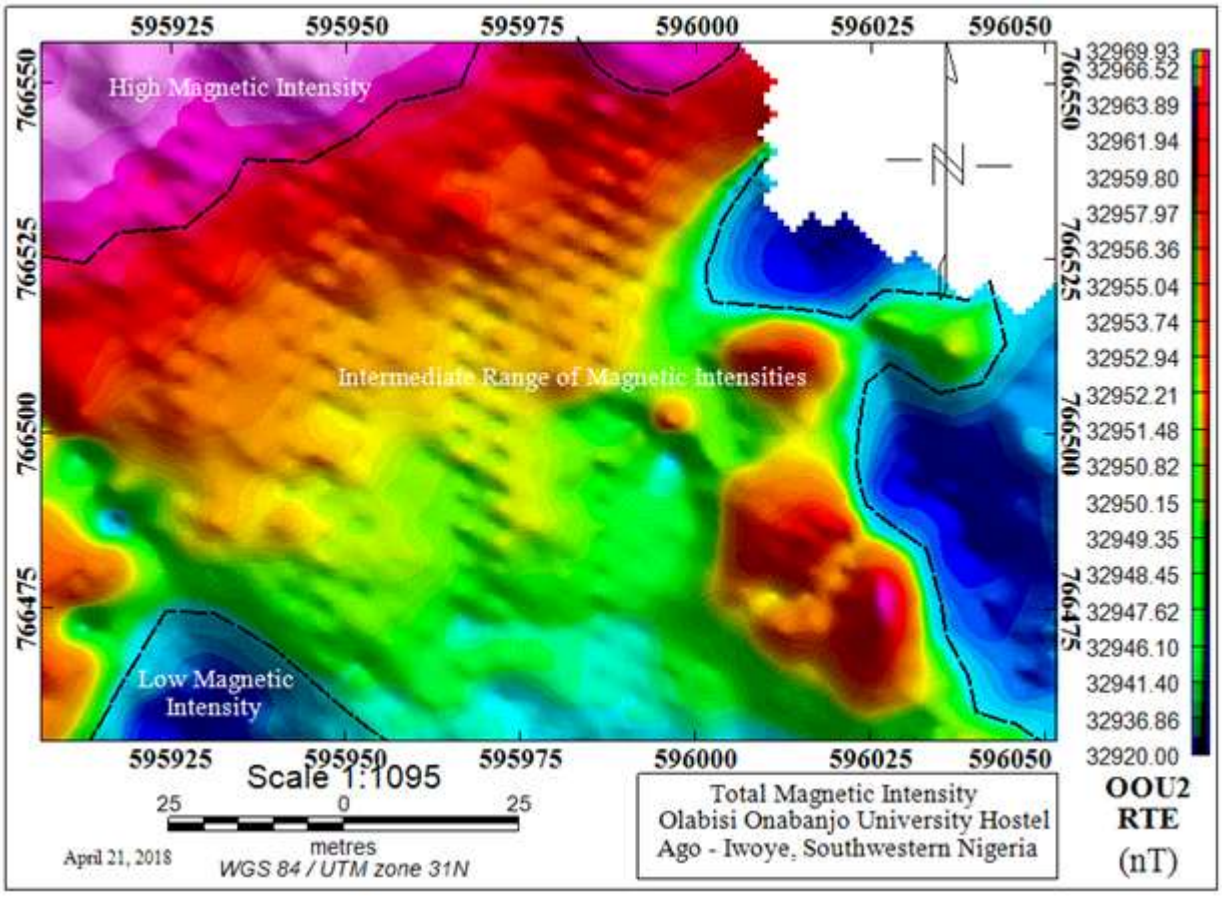

Figure 8. Total Magnetic Intensity Map of Location B. The map depicts the spatial variation in resultant intensity induced by short and long wavelength magnetic sources in the area. Magnetic intensities decrease diagonally from northwest down south, while exhibiting an anomalous intensity contrast around the eastern and the south-western part

Volume 66 (2020), No. 1
p. 1–32, ISSN 1802-5420
DOI 10.35180/gse-2020-0027

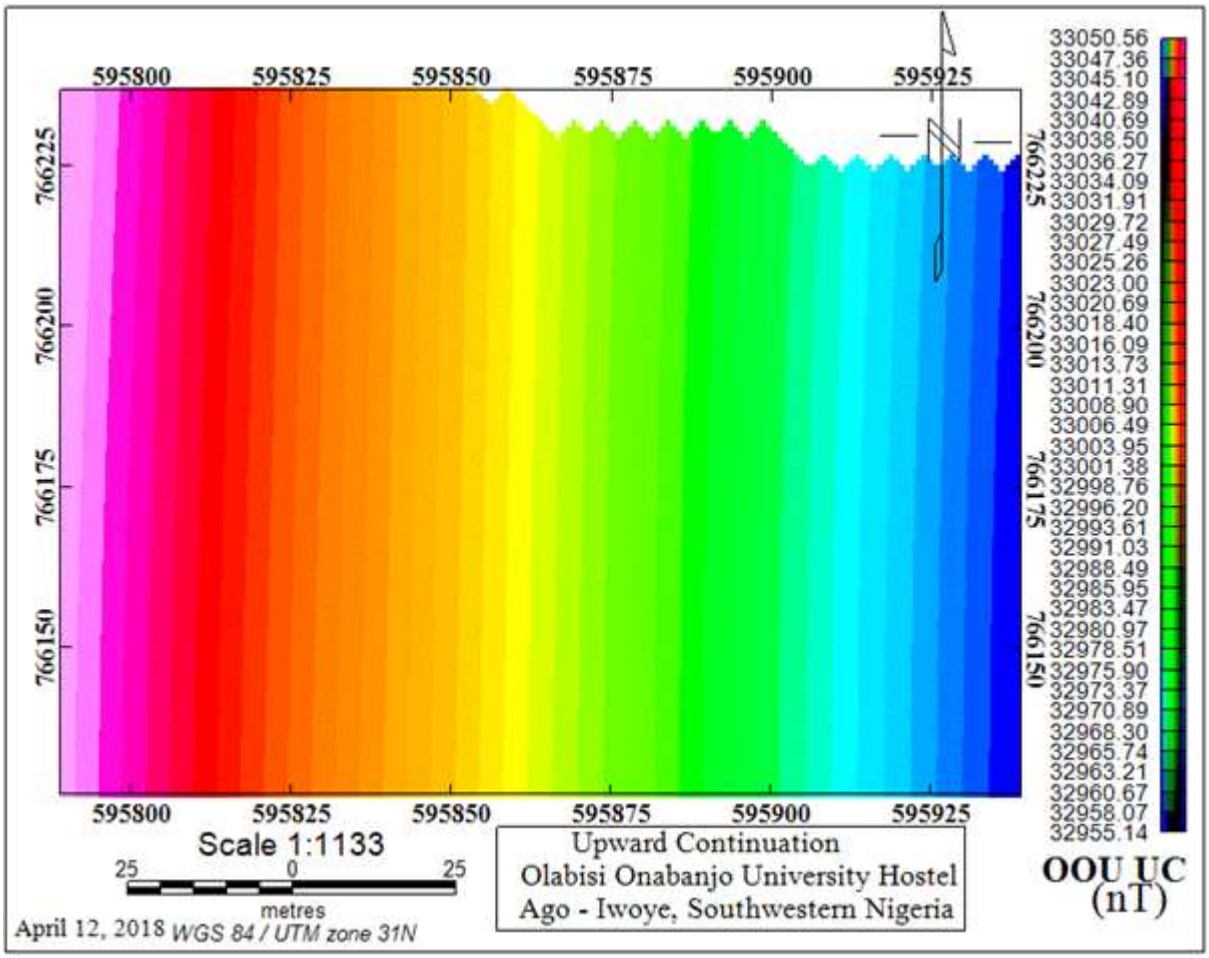

Figure 9. Regional Magnetic Intensity Map of Location A. Computation for magnitude and trend of the regional magnetic field was achieved using the upward continuation process. The process truncates any wavelength component below a cut-off threshold of 80m in the filter to generate the long wavelength components of the total field, which also exhibits an east-west decrement trend

Volume 66 (2020), No. 1
p. 1–32, ISSN 1802-5420
DOI 10.35180/gse-2020-0027

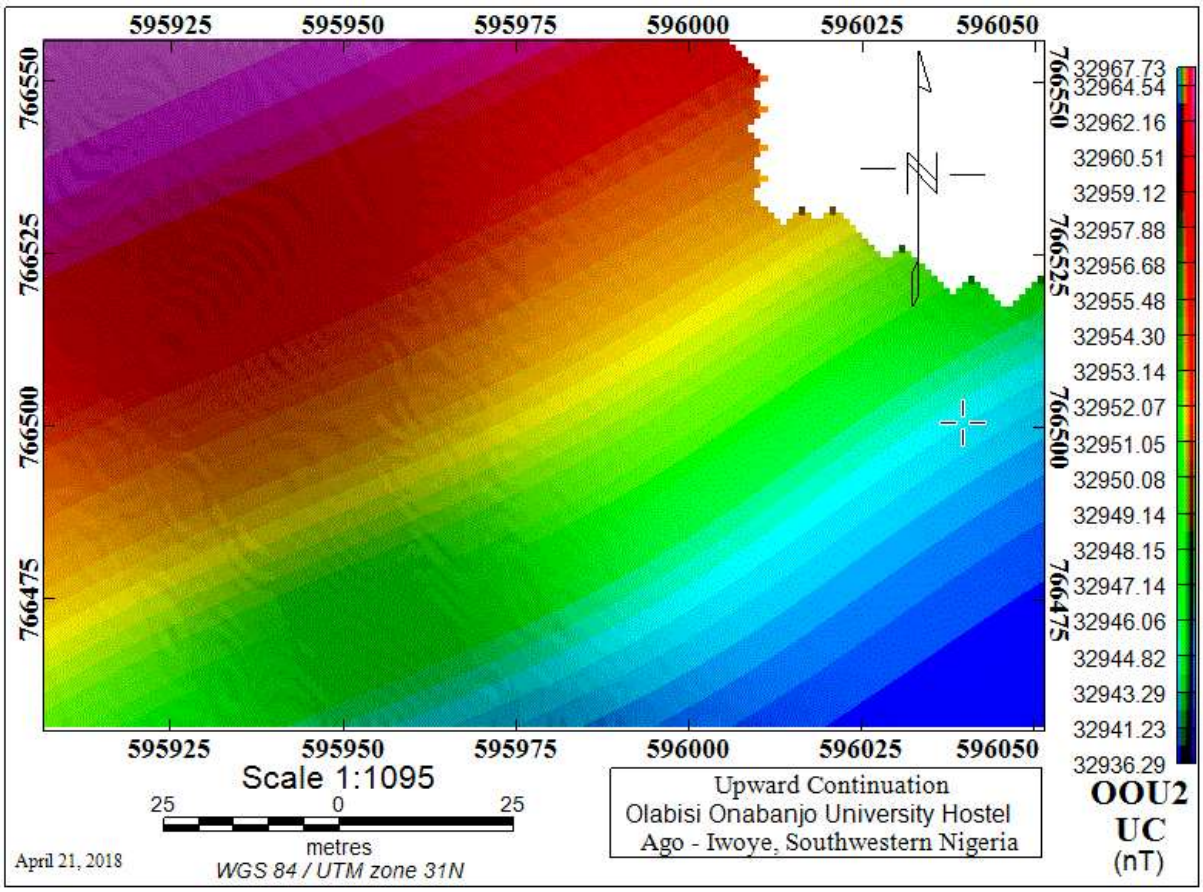

Figure 10. Regional Magnetic Intensity Map of Location B. Observed northwest-southeast decrement trend of long wavelength component was computed using the upward continuation process to a depth of 80m

Both the conventional residual anomaly map and its derivatives are essential for geological and structural interpretation, and hence inferences from various generated maps are integrated for a better comprehensive interpretation. The anticipated use of the first and second vertical derivatives is unnecessary for the shallowly located magnetic sources as any further accentuations may result in the blurring and disruption of magnetic signals.

7 RESIDUAL MAPS

Magnetic anomalies depicted in the magnetic maps of the area (Figures 11 and 12) are essentially of the steep gradient linear low intensity type, low intensity magnetic closures, and high intensity magnetic closures. Linear low magnetic intensity anomalies crosscutting the granite gneiss complex are structural expressions of linear discontinuities, which on the first grid runs NW– SE but with a little shift in strike azimuth on the second grid. The circular low closures could either be reflection of relatively deeper location of magnetic sources or a contrasting lithological zone composed of felsic minerals, but vice versa for high intensity magnetic closures (an ambiguity resolved using the analytical signal). Aside the anomalies, unremarkable quiet magnetic zones are also well outlined in this map, more distinctive as pseudo-circular magnetic bodies at location B.

Volume 66 (2020), No. 1
p. 1–32, ISSN 1802-5420
DOI 10.35180/gse-2020-0027

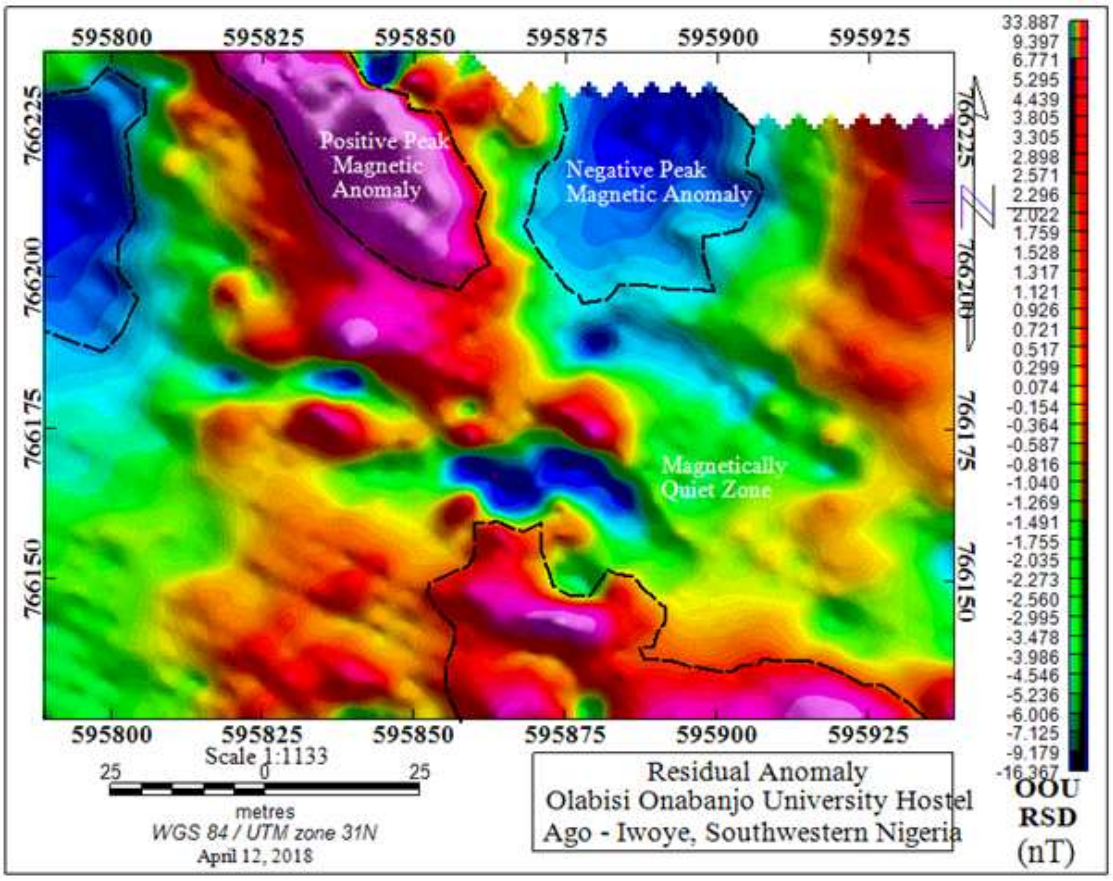

Figure 11. Residual Anomaly Map of Location A. Outlined zones on the map depicts areas of high (violet) and lows (blue) magnetic residuals which could either indicate variation in depth of occurrences of geologic bodies or compositional variability. The most striking anomalies on this occur around the central part as long linear negative magnetic body crosscutting a narrowly separated high magnetic blocks. This high gradient anomaly and other associated types on the map are inferred as fractures within the granite gneisses

Volume 66 (2020), No. 1
p. 1–32, ISSN 1802-5420
DOI 10.35180/gse-2020-0027

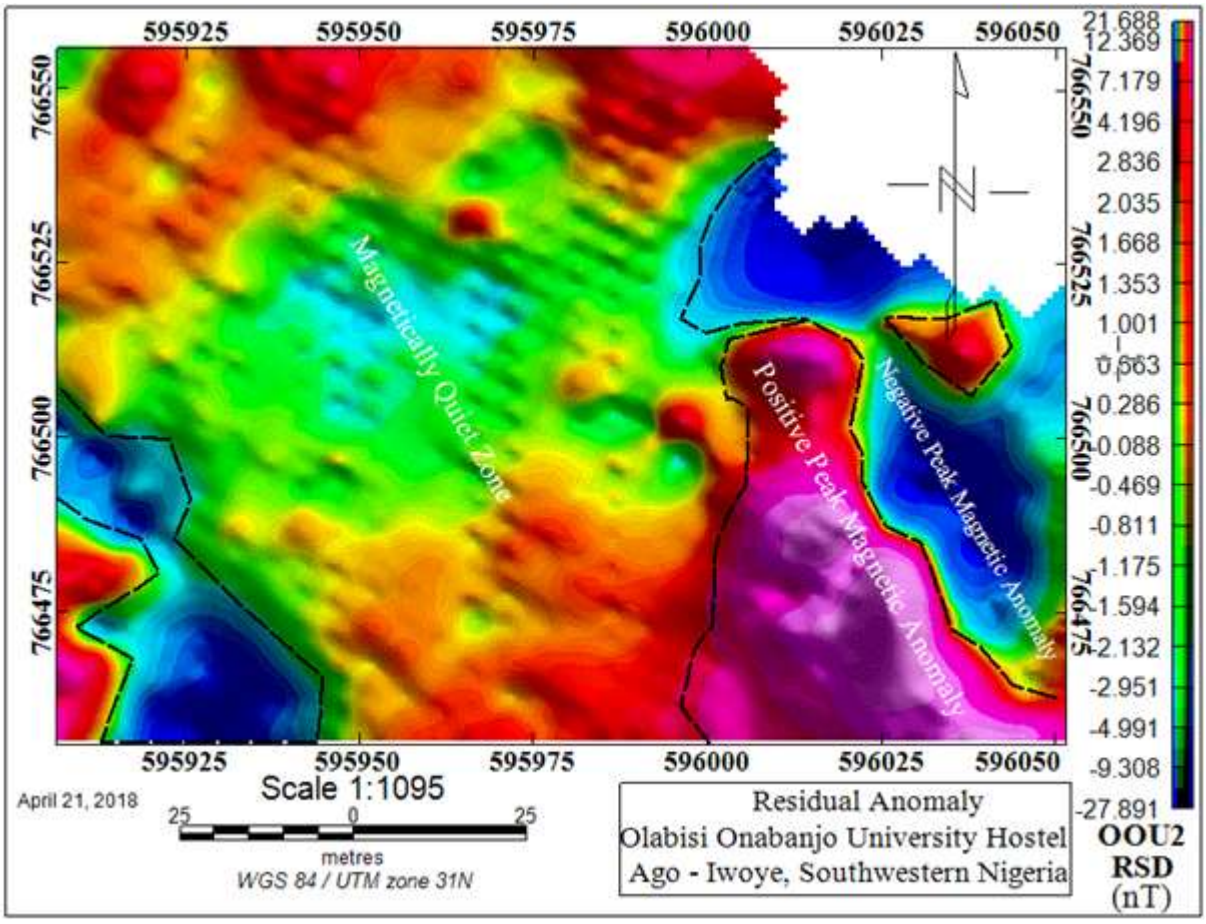

Figure 12. Residual Anomaly Map of Location B. On a relative scale, larger part of this location is magnetically quiet when compared to location A. However, steep susceptibility gradient is noticeable along the eastern boundary and south-western corner between the high (violet) positive peaks and the low (blue) negatives peaks due to the occurrence of a buried microlin (local fracture)

8 ANALYTICAL SIGNAL MAPS

Analytical signal amplitude maxima are uniquely recorded at the edges of anomalous magnetic bodies irrespective of direction of magnetization [10, 11,12, 13], and as highly effective for source edges detection. Edges of inducing source bodies are readily identified by their anomalously high amplitude characteristics on the analytical signal maps (Figures 13 and 14). Signal response of magnetic source elements is contrastingly high along structural discontinuities within the rock but relatively weak over the undeformed segments of the bedrock. No lithological heterogeneity is observable in both analytical signal maps of both locations; an indicative of a fairly uniform subsurface geology across the study locations. In view of these similar susceptibility responses of the gneisses, positive and negative magnetic closures delineated in the residual map are believed to be topographic expression of buried basement peaks and depression, as against the contending inference of compositional heterogeneity.

Volume 66 (2020), No. 1
p. 1–32, ISSN 1802-5420
DOI 10.35180/gse-2020-0027

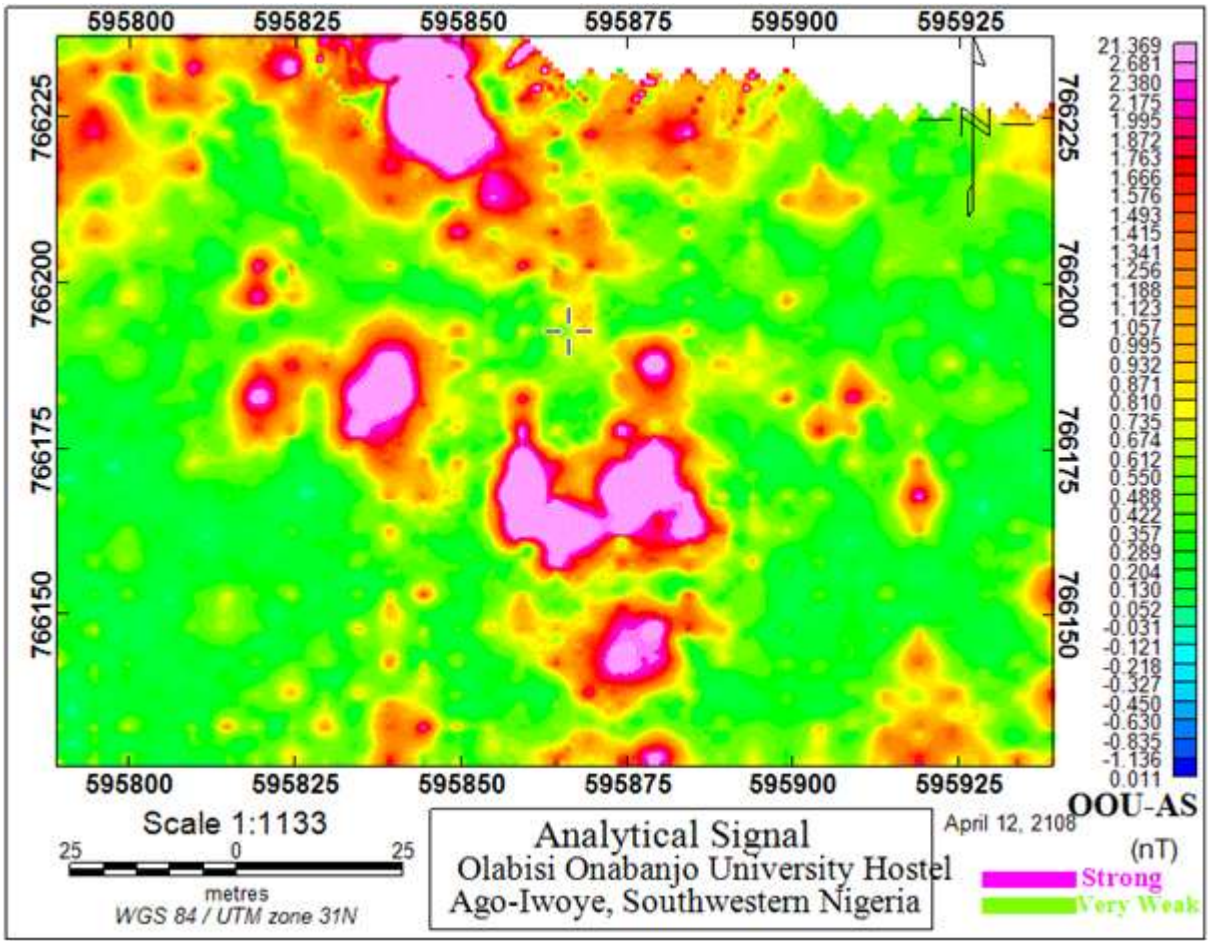

Figure 13. Analytical Signal Map of Location A. Zones of high analytical signal amplitude (signified by the violet patches) not only indicate the presence of anomalies but also outline the edges inducing magnetizing body irrespective of the direction of magnetization. Background signal amplitude (lemon green) of the gneiss covers a substantial portion of this location

Volume 66 (2020), No. 1
p. 1–32, ISSN 1802-5420
DOI 10.35180/gse-2020-0027

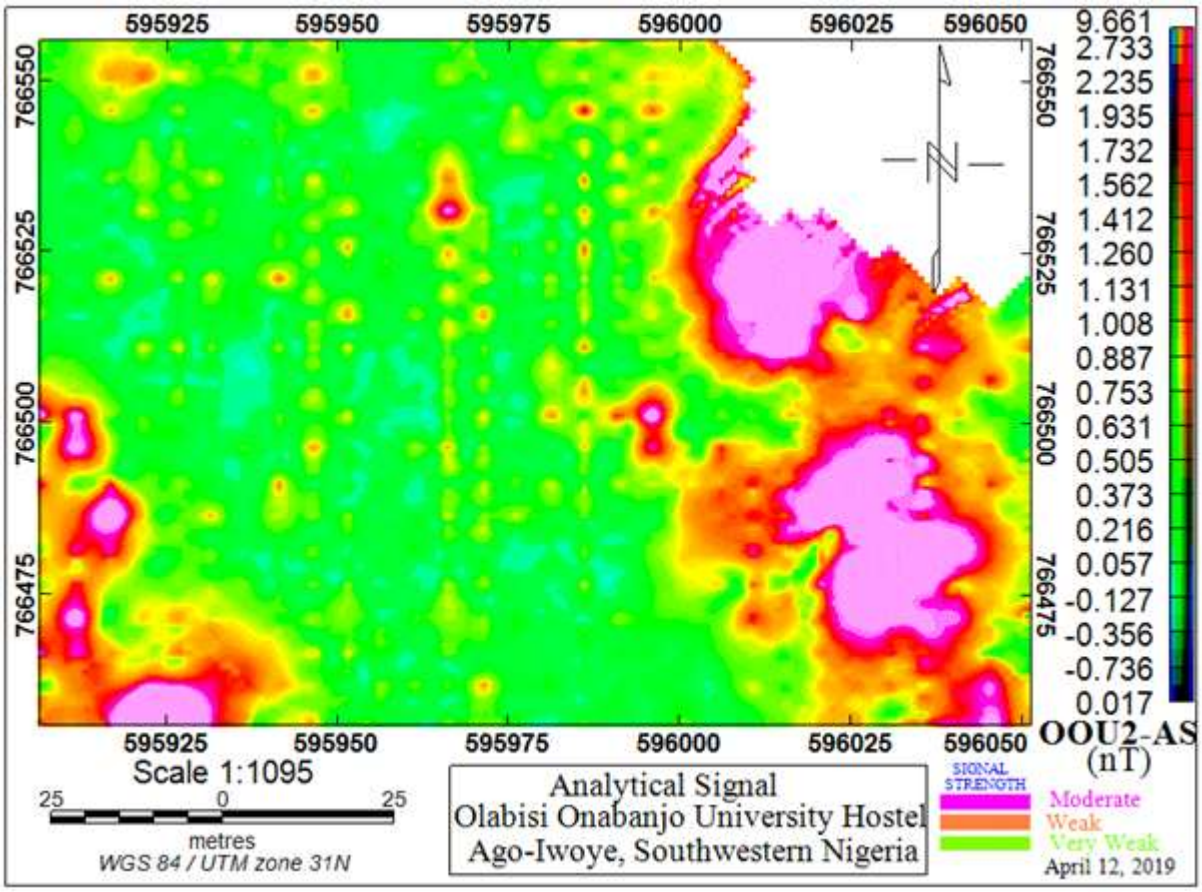

Figure 14. Analytical Signal Map of Location B. Location of the causative bodies of the observed anomalies (violet) on the eastern and south-western margin are clearly distinguished on the basis of contrasting higher signal amplitude characteristics than that of the background of the analytical signal map. Geometry of these magnetic sources are somewhat elongated in NNW – SSE direction

9 TILT ANGLE DERIVATIVE MAPS

Tilt angle derivative is an effective edge detection tool based on the equalization of magnetic anomalies amplitudes for the accentuation of weak prominent sources [14]. The filter permits the discrimination of short amplitude waveforms from the high amplitude ones associated with magnetic anomalies, thus, very useful for the delineation of linear geological or geomorphological structures without necessarily suppressing the long-wavelength components [15, 16]. Positive magnetic elements on the TDR maps (Figures 15 and 16) directly reveal the location of concealed inducing geological bodies, and whose edge geometries, as spatially defined by the zero gradient contours, approximately exhibit elongated structural fabrics. Extreme negative derivatives exhibit two distinct geometrical forms; firstly, as roughly circular hollow over the relatively overburden laden bedrock depressions, and along the high gradient areas (intersection spots between the positive peaks and the negative troughs) as elongated weakness within the basement structural discontinuities. Fracture azimuths of magnetic bodies vary spatially in the area; aligning predominantly in the NE - SW direction at location A, and an ‘X’ structural junction of NNE – SSW and NE – SW at location B.

Volume 66 (2020), No. 1
p. 1–32, ISSN 1802-5420
DOI 10.35180/gse-2020-0027

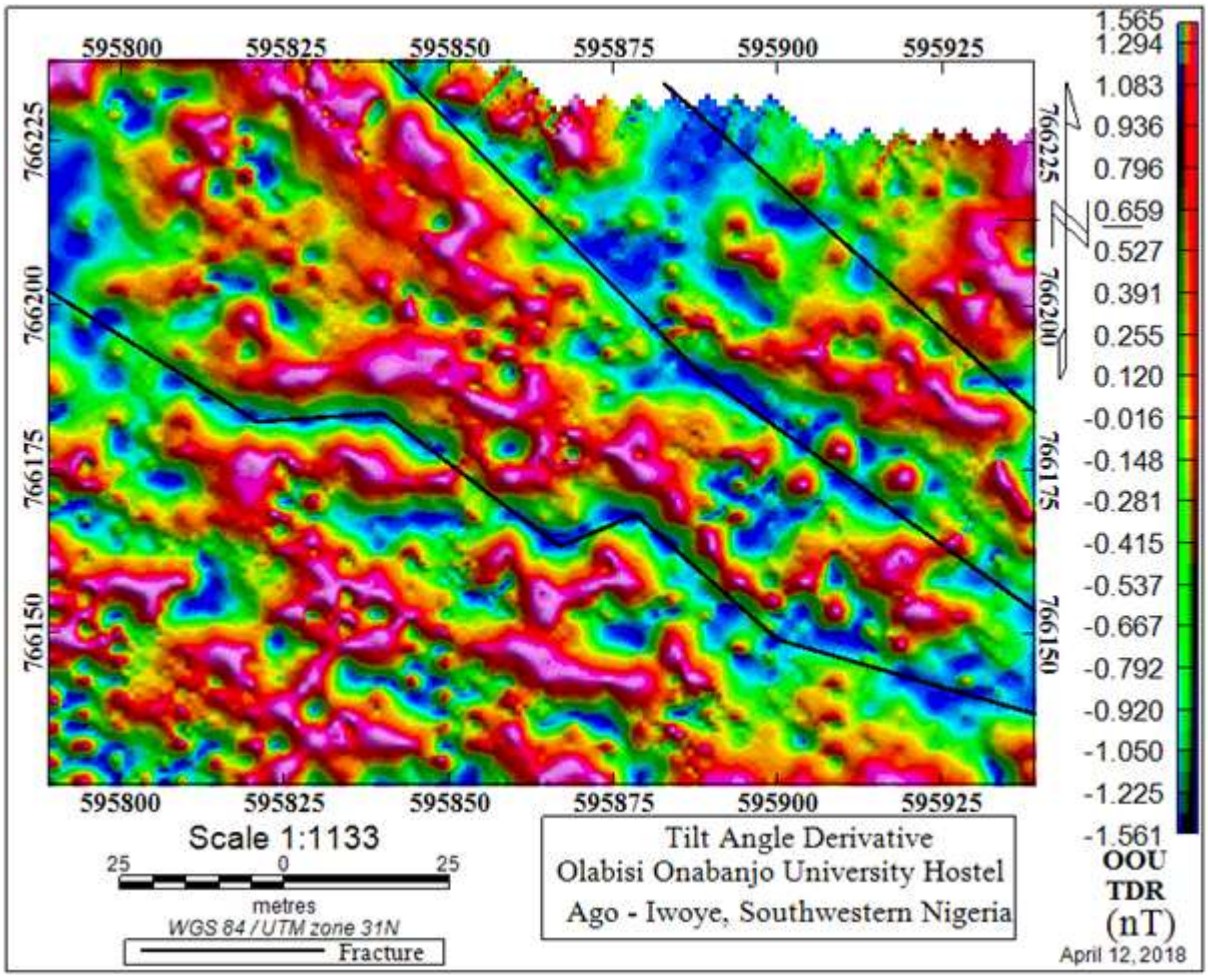

Figure 15. Tilt Derivative Map of Location A. Three subparallel NW – SE trending magnetic microlins (dark lines) are apparently revealed along the abrupt source boundary between the positive (violet) and negative (blue) anomalies in the map; conservatively inferred as structural discontinuities within the gneisses. The terminology 'microlin' simply refers to any micro-linear or linear geological structure with restricted or localized extent, and whose aspect ratio in term of length/width is ≥20 but ≤100. Such description is needed in magnetic map interpretation to distinguish microstructures from megastructures

Volume 66 (2020), No. 1
p. 1–32, ISSN 1802-5420
DOI 10.35180/gse-2020-0027

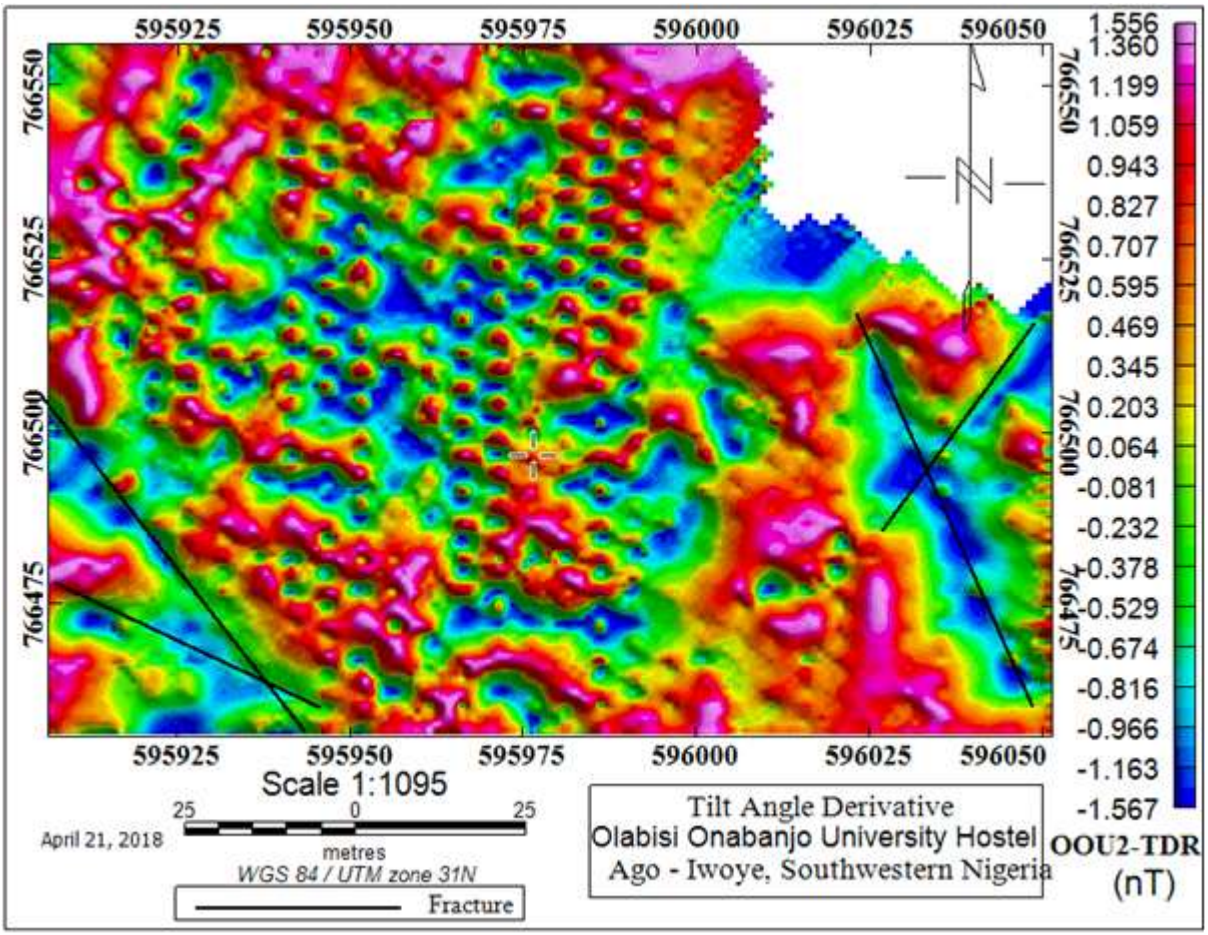

Figure 16. Tilt Derivative Map of Location B. Leading edges of magnetic bodies along the eastern and the south-western part are well detected in this map. Identified magnetic microlins (dark lines) coincide with the elongated negative amplitude anomalies of the shallowly buried crosscutting fractures. Trend of deformation is NW-SE, NNW-SSE and NE-SW

10 POWER SPECTRUM

Average depth estimates of magnetic sources can be roughly calculated from the wavelength signature of a power spectrum [17]. Depth parameters proffered by power spectrum depend on geometrical characteristics (amplitude, wavelength and frequency) of the waveform. Figures 17 and 18 are power spectra of magnetic sources at location A in one and two dimension respectively. A maximum amplitude of 0.17k-unit (Figure 17) was recorded close to the graph's origin; diminished drastically to 0.04k-unit at 60, and from this point fluctuated between 0 and 0.05k-unit to the end of the spectrum. This signature corresponds to a depth range of 1m – 12m on the 2-D power spectrum (Figure 18).

Volume 66 (2020), No. 1
p. 1–32, ISSN 1802-5420
DOI 10.35180/gse-2020-0027

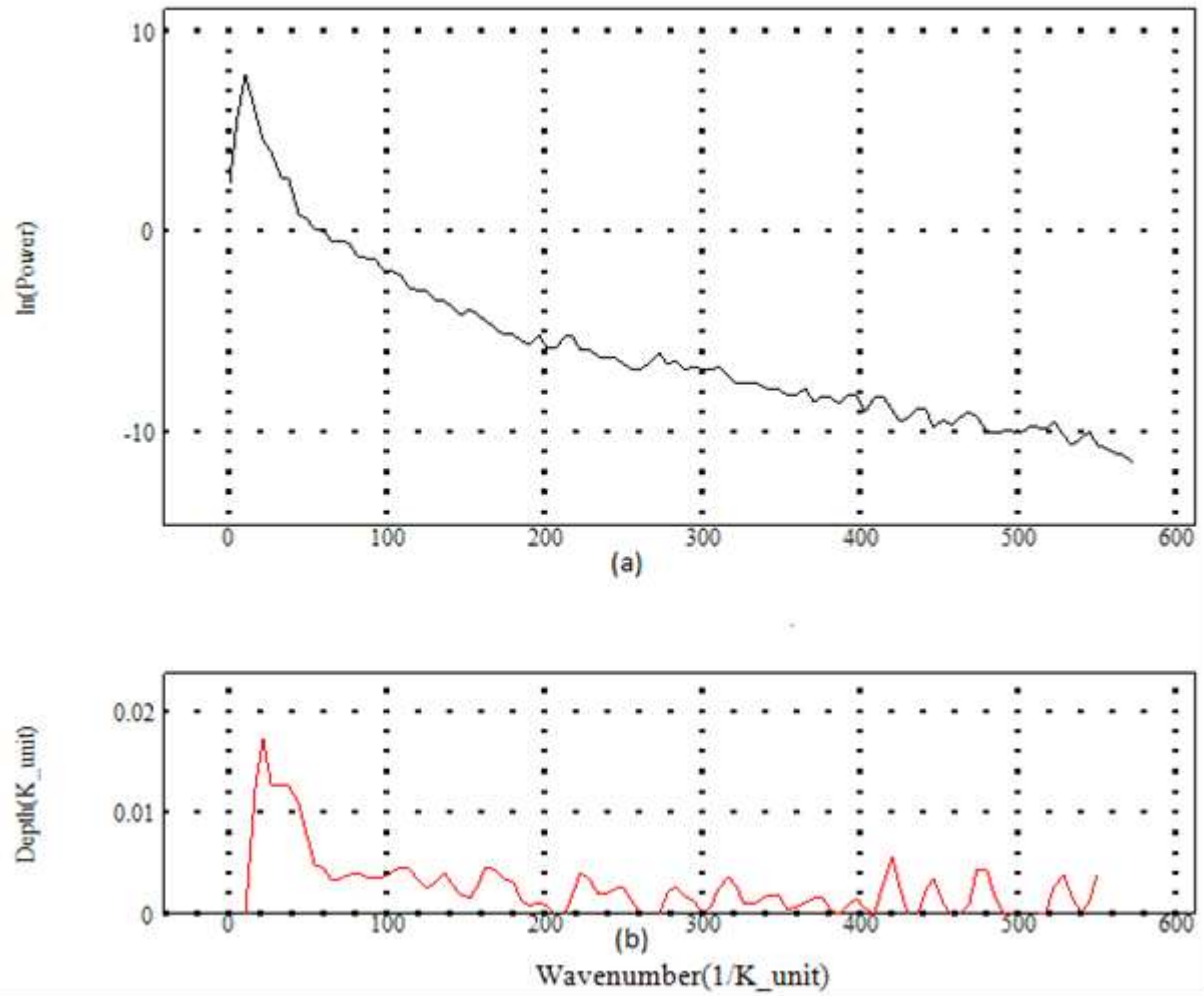

Figure 17. Radially Averaged Power Spectrum of Magnetic Sources at Location A. (a) Plot of power against wavenumber reveals a spectrum signature characterized by strong signal amplitude around the origin (0 – 60) which diminishes steadily between 60 and 200, and broad weak signal amplitude between 200 and 600. (b) Plot of depth against wavenumber depicts the occurrences very short wavelength anomalies with strong magnetization between 0 and 60, and a rather extensive series of longer wavelength lobes associated with deeper sources and weaker magnetization effects

Volume 66 (2020), No. 1
p. 1–32, ISSN 1802-5420
DOI 10.35180/gse-2020-0027

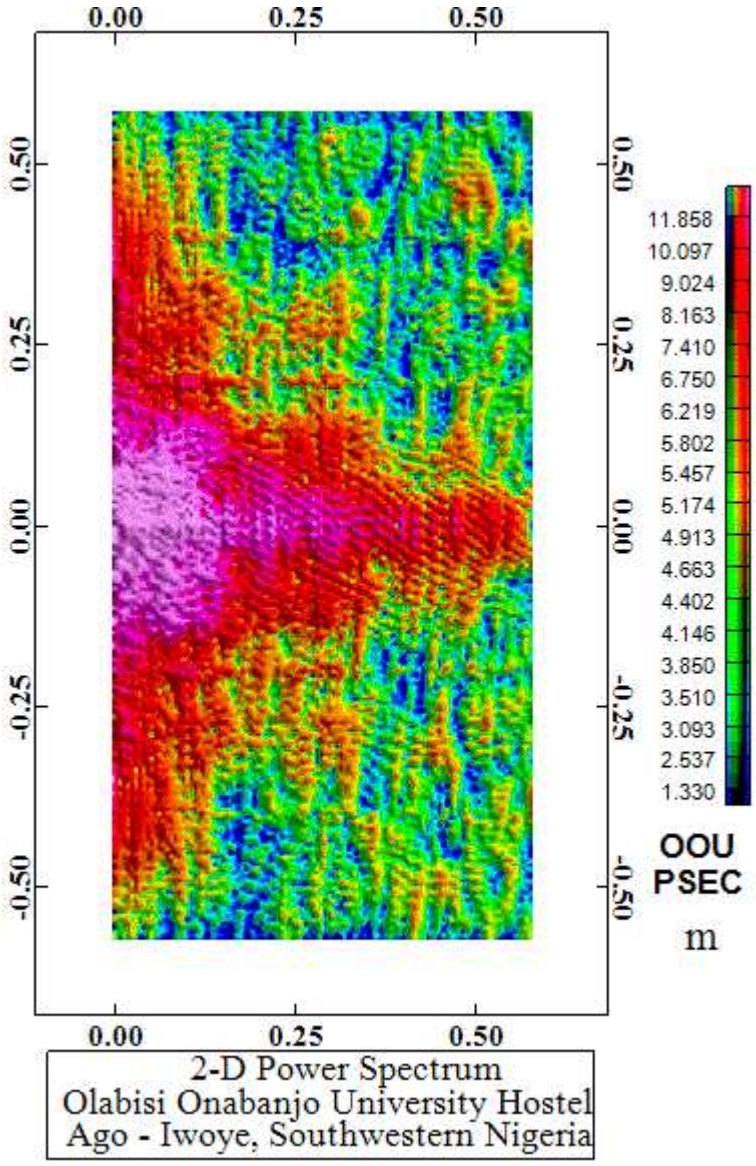

Figure 18. Two Dimensional Power Spectrum of Location A

The spectrum pattern recorded at location B differed significantly. Here, amplitude decreased irregularly from 0.009k-unit around the origin to 0k-unit at 2001/k-unit (Figure 19), and from the later position, amplitude fluctuations ranged between 0k-unit and 0.003k-unit, corresponding to a depth range of 0 to 22m on the 2-D power spectrum (Figure 20). From the spectra analyses of both locations, average signal amplitude is stronger at location A than B, but contra wise in terms of wavelength attributes – being shorter at location A than B.

Volume 66 (2020), No. 1
p. 1–32, ISSN 1802-5420
DOI 10.35180/gse-2020-0027

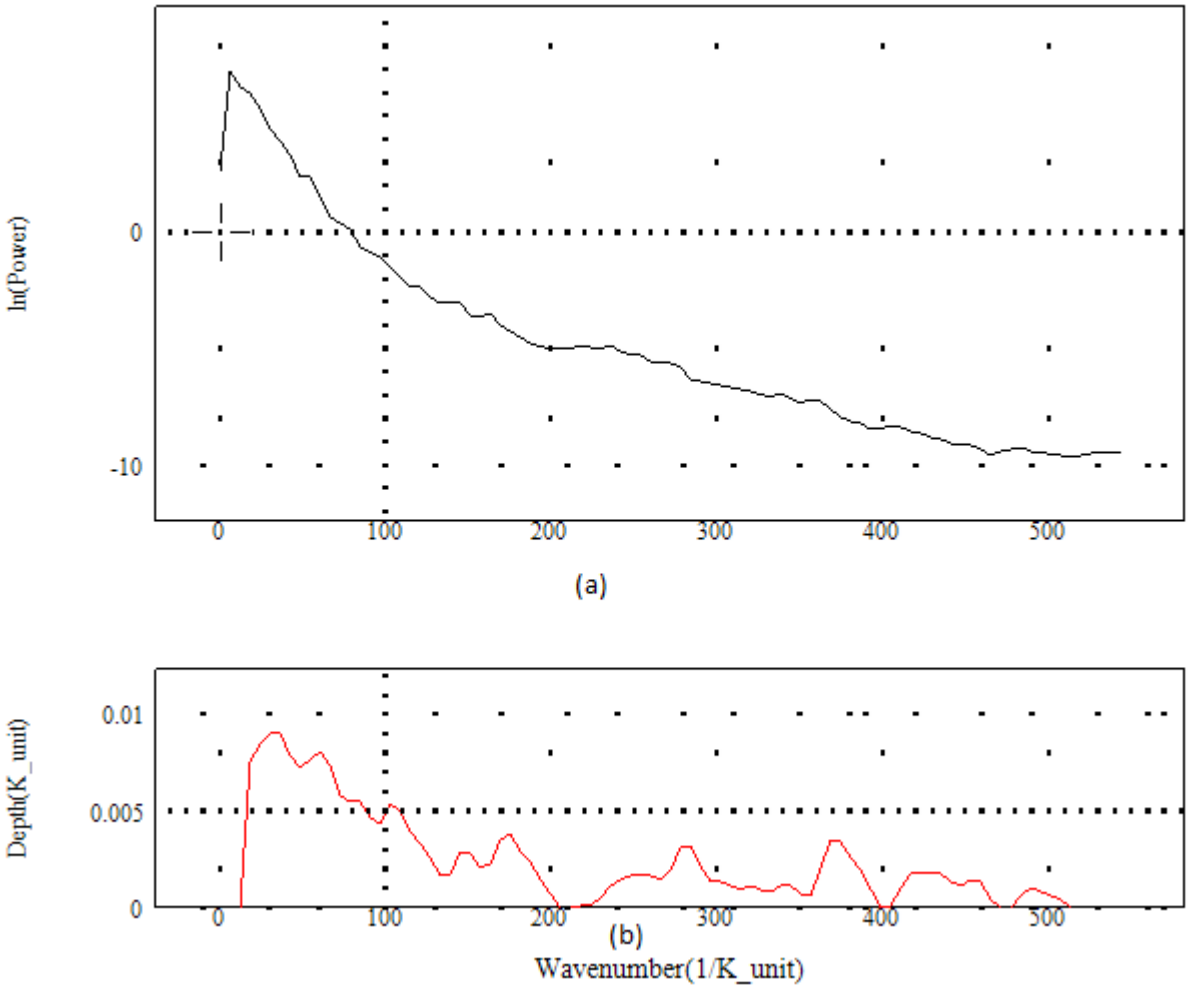

Figure 19. Radially Average Power Spectrum of Magnetic Sources at Location B. (a) Plot of power against wavenumber; revealing a continuous drop in signal amplitude from the origin to the end of the signature due to diverse source characteristics. (b) Superimposition of short wavelength anomalies on their long wavelength components is discernible on the plot of depth against wavenumber

Volume 66 (2020), No. 1
p. 1–32, ISSN 1802-5420
DOI 10.35180/gse-2020-0027

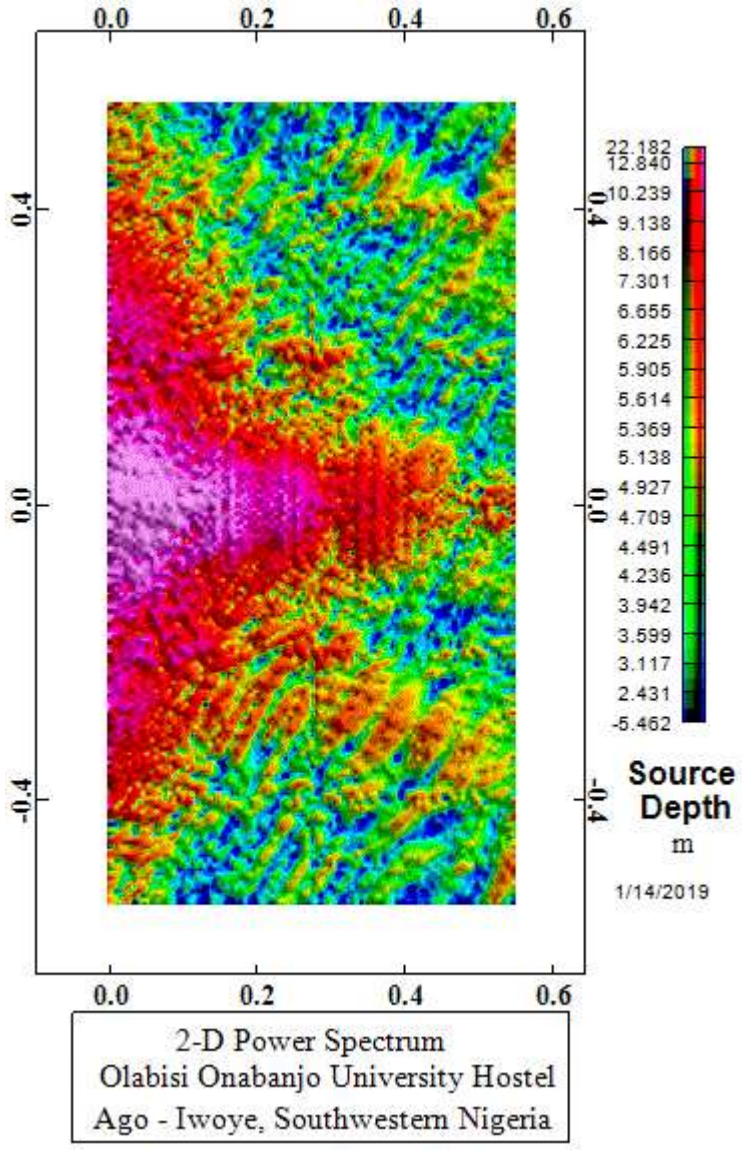

Figure 20. Two Dimensional Power Spectrum of Location B

11 EULER DECONVOLUTION MAPS

A structural index (S.I) of 1.0 is considered the most useful Euler solution for the depth characterization of the magnetic anomalies since its geometric assumption could be linear or inclined, and the genetic projection of anomalies is intrusive [18]. Dyke or sill model (S.I = 1.0) is also valid for geological structures because the emplacement of intrusive bodies is structurally controlled. Located Euler 3D deconvolution (Figures 21 and 22) presents a far accurate mechanism for the depth estimate of spatially located magnetic sources. Elevation of source bodies ranges between 39m for deepest sources and 49m for the shallowest; reflecting a maximum 10m relief irregularity within the bedrock, and a corresponding maximum overburden thickness of 10m. Although the bedrock is contorted by random depressions, the resultant warp tilt south easterly is in consistence with the surface topography. Regolith cover is relatively thicker within the depression but expectedly very thin on the platform.

Volume 66 (2020), No. 1
p. 1–32, ISSN 1802-5420
DOI 10.35180/gse-2020-0027

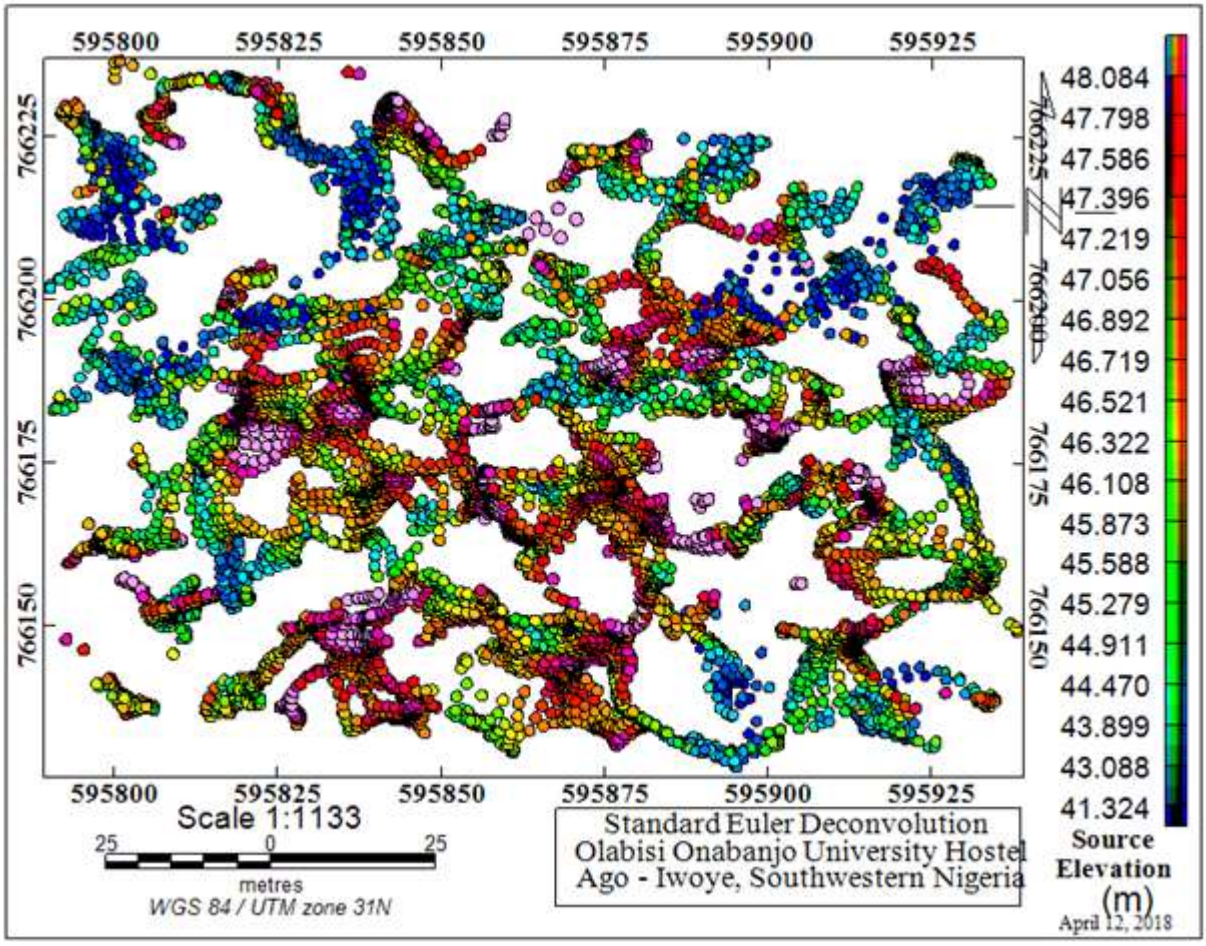

Figure 21. Euler Deconvolution Plot for Location A using a structural index of 1.0. Elevation model was adopted for depth estimation; an average surface elevation of 50m was assumed. The solid circles denote the depth of occurrences of inducing bodies. Colour blue for source depth >10m, green for depth range of 4m – 7m, red ranges between 2m – 3m and violet <2m. A crab eye's view of the subsurface recognized different topographic irregularities comprising of basement platforms and depressions

Volume 66 (2020), No. 1
p. 1–32, ISSN 1802-5420
DOI 10.35180/gse-2020-0027

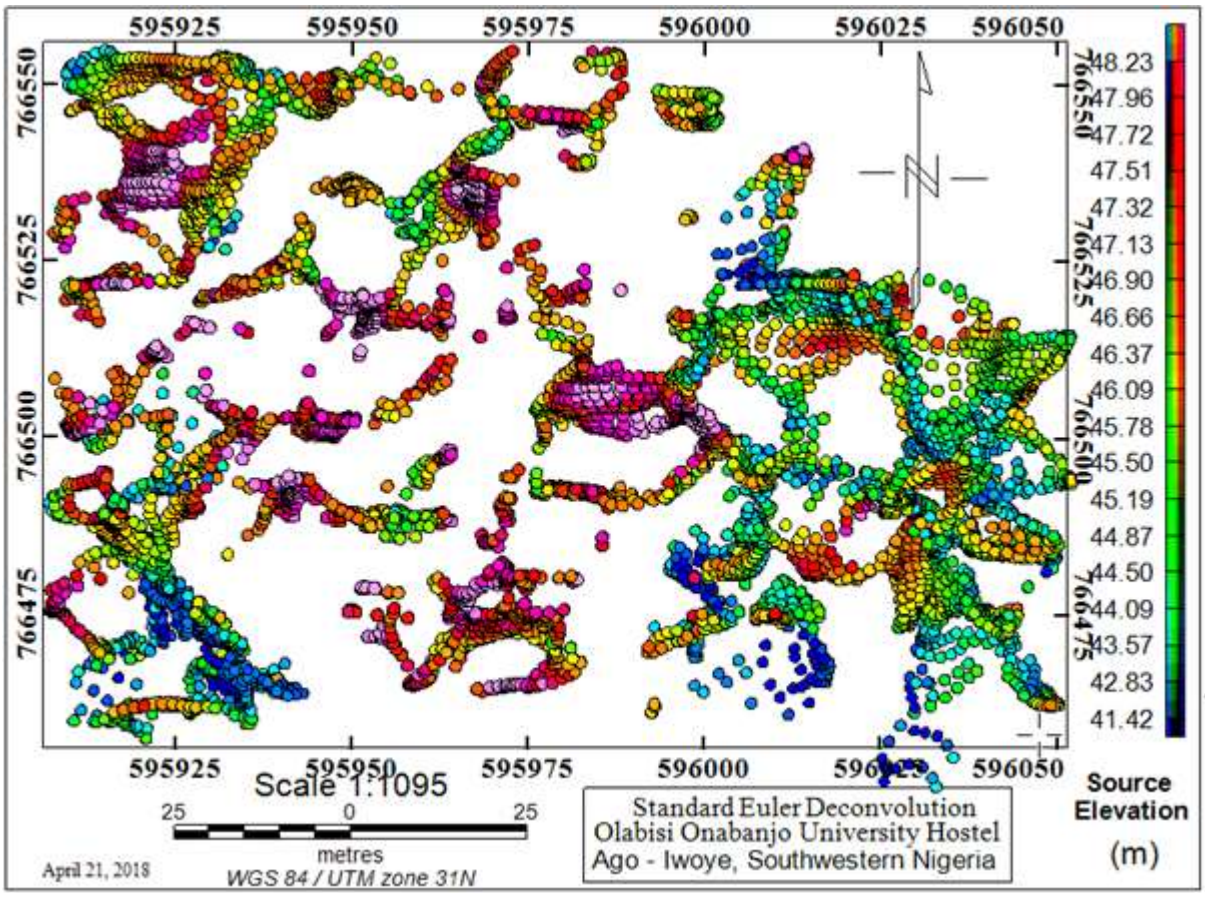

Figure 22. Euler Deconvolution Plot for Location B using a Structural Index of 1.0. Solid circle denotations in the map include blue, green, orange and red for depth range >10m, between5m – 8m, 3m – 5m and <2m

12 COMPOSITE MAGNETIC MAPS

Combining the tilt angle derivate map and the residual anomaly map generated a coherent composite magnetic map (Figures 23 and 24) depicting a very strong overlay correlation, more remarkably around source edges contact which more clearly revealed the continuity of structural discontinuities with the study terrain. The second composite map (Figures 25 and 26) is a superimposition of tilt angle derivative structures on Euler deconvolution map to discriminate between the delineated fractures as either bedrock joints or faults. Examination of these structural positions on the bedrock topography confirms location 'A' and 'B' as a jointed and faulted spots respectively.

At location A (Figures 25), all the delineated structures are inferred as bedrock joints, exhibiting a NW – SE orientation across the central bedrock platform and depressions, and almost at parallel angle to one another. Deformation history of this area can be closely connected to the NE – SW perpendicular stress impact exerted on the rock bodies; synonymous with the orogenic episodes during the Liberian age. Structural settings differ slightly at location B (Figures 26). Fracture azimuths coincide directly with elongated depressions bounding the edges of juxtaposed magnetic sources, which evidently suggests dip slip displacement of basement blocks. Faulting pattern is normal with an estimated throw of 4.5 m (Figures 26). Basement reactivation during the Pan-African orogeny rejuvenated a relatively weaker stress regime that aggravated a NE – SW converse structural discontinuity, cross-cutting the older structures to create an 'X' fracture junction on the eastern pattern of the location B. However, the resultant fracture direction is NW-SE.

Volume 66 (2020), No. 1
p. 1–32, ISSN 1802-5420
DOI 10.35180/gse-2020-0027

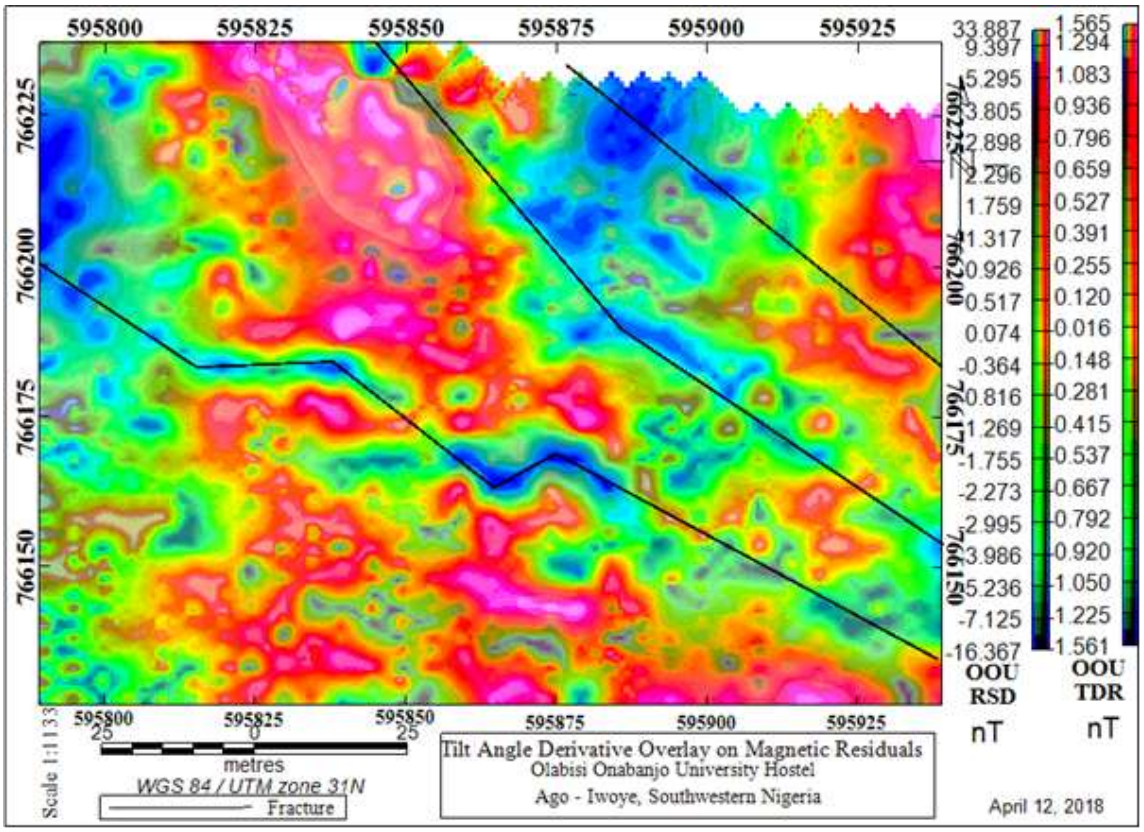

Figure 23. Overlay of Tilt Derivative Map and Residual Anomaly Map of Location A. Microlins on the tilt derivative map directly coincide with the negative anomalies on the residual anomaly map, hence, the negative anomalies are structurally induced, while the positives indicate the spatial occurrences of geological blocks

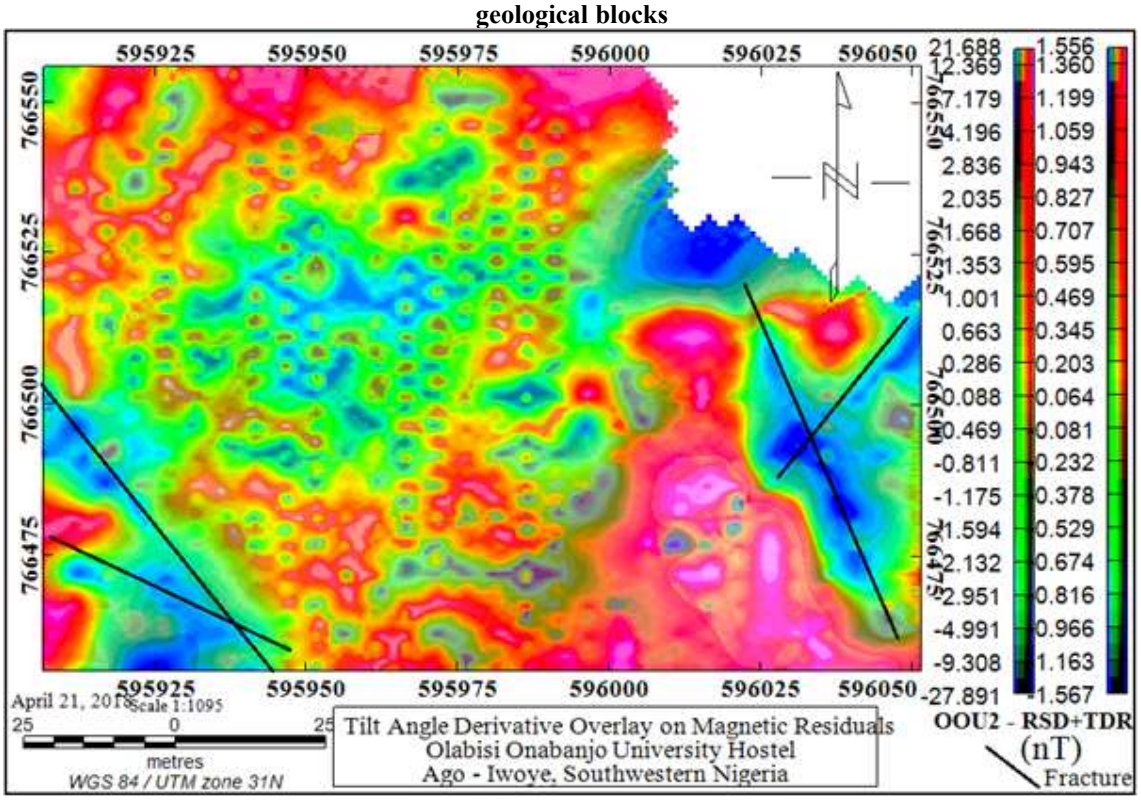

Figure 24. Overlay of Tilt Derivative Map and Residual Anomaly Map of Location B. Microlins also align along the negative anomalies, affirming the structural inducement of the negative anomalies. Positive anomalies are indications of geological responses of buried migmatite-gneiss complex

Volume 66 (2020), No. 1
p. 1–32, ISSN 1802-5420
DOI 10.35180/gse-2020-0027

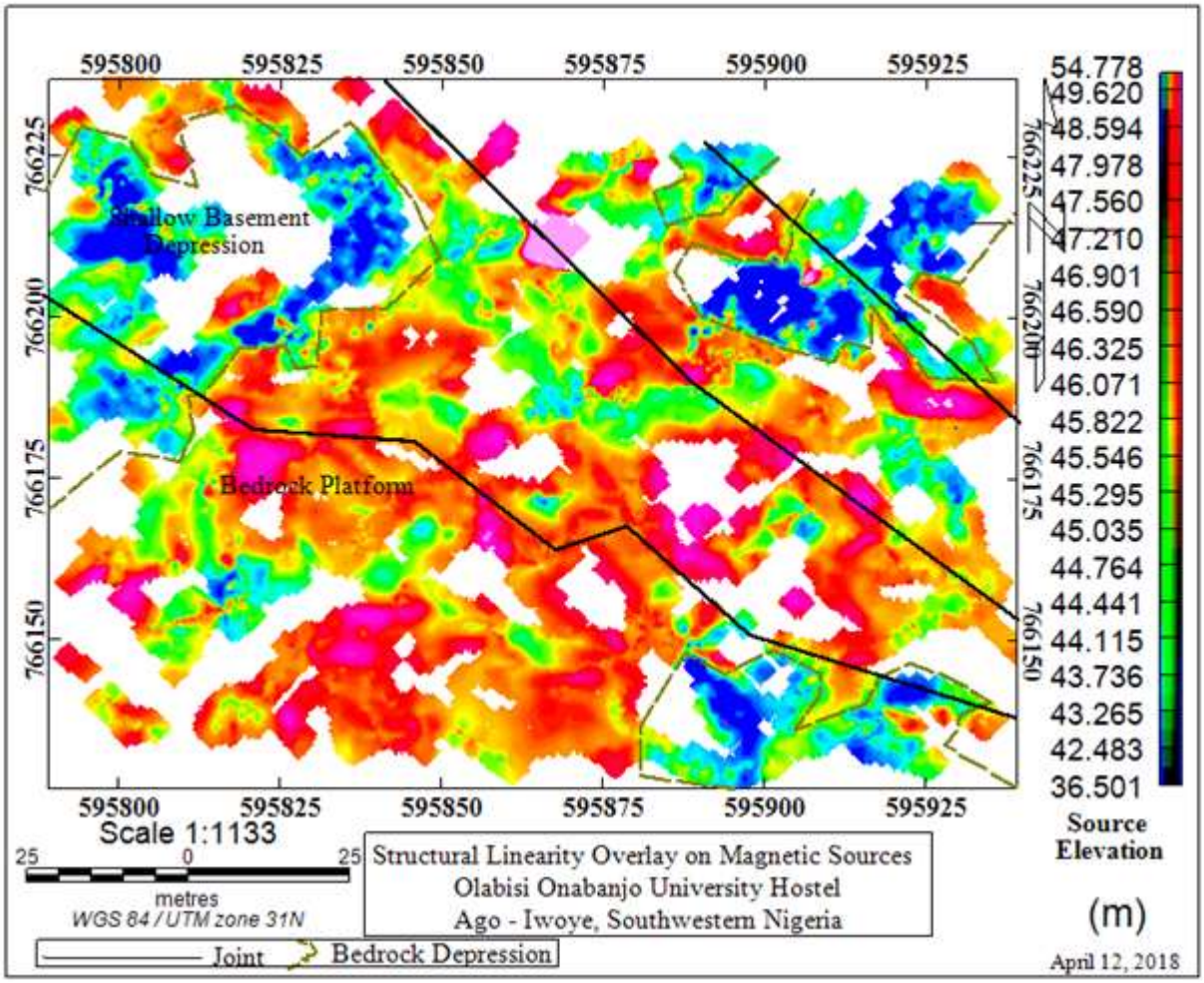

Figure 25. Overlay of Tilt Derivative Map and Euler Deconvolution Map of Location A. This amalgamation is imperative for the distinction between a basement depression and the footwall of a faulted geological unit. In this instance, microlins dissect both the shallow (red/violet) and deeper (blue) magnetic sources, which in accordance to the 'principle of cross cutting relationship' indicate a younger (brittle) deformation event on the existing buried basement configuration. Thus, the sub-circular blue zones are jointed basement depressions

Volume 66 (2020), No. 1
p. 1–32, ISSN 1802-5420
DOI 10.35180/gse-2020-0027

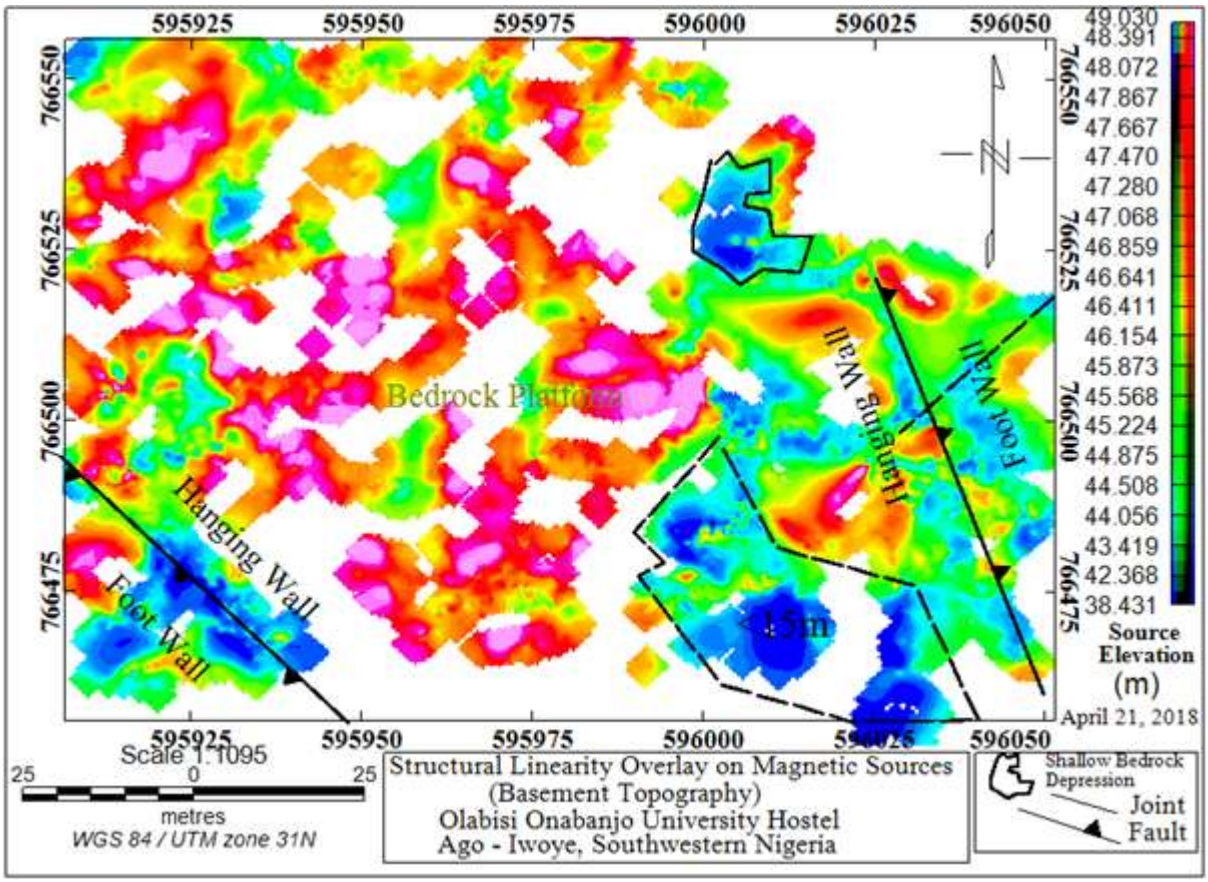

Figure 26. Overlay of Tilt Derivative Map and Residual Anomaly Map of Location B. Euler map depicts a magnetic source architecture composed of very shallow (violet coded) sources, and a relatively deeper (green and blue coded) sources. An overlay of tilt derivative identified faulted zones on the eastern western boundaries

13 MAGNETIC PROFILING

An easier mechanism for the visualization of magnetic anomalies commonly entails the use of magnetic profiles. Total magnetic intensity distributions (32994nT – 33046nT) across the regional field (32997nT – 33019nT) along profile A (Figure 27) recorded prominent anomalies which were noticeably distinct as negative (-11nT) and positive (30nT) magnetic lobes between distance 30m – 45m and 85m – 100m due to the marked presence of structural discontinuity and basement block proximity to the surface respectively. Peak analytical signals of 4.7nT and 10.4nT were recorded over the anomalies (Figure 28).

Maximum range of total and regional intensity value along profile B was 32927nT – 32957nT and 32943nT- 32945nT in that order (Figure 27). Anomaly curve along this profile (Figure 28) was a rather magnetic spike of 30nT with a corresponding maximum signal of about 5nT induced by block discontinuity.

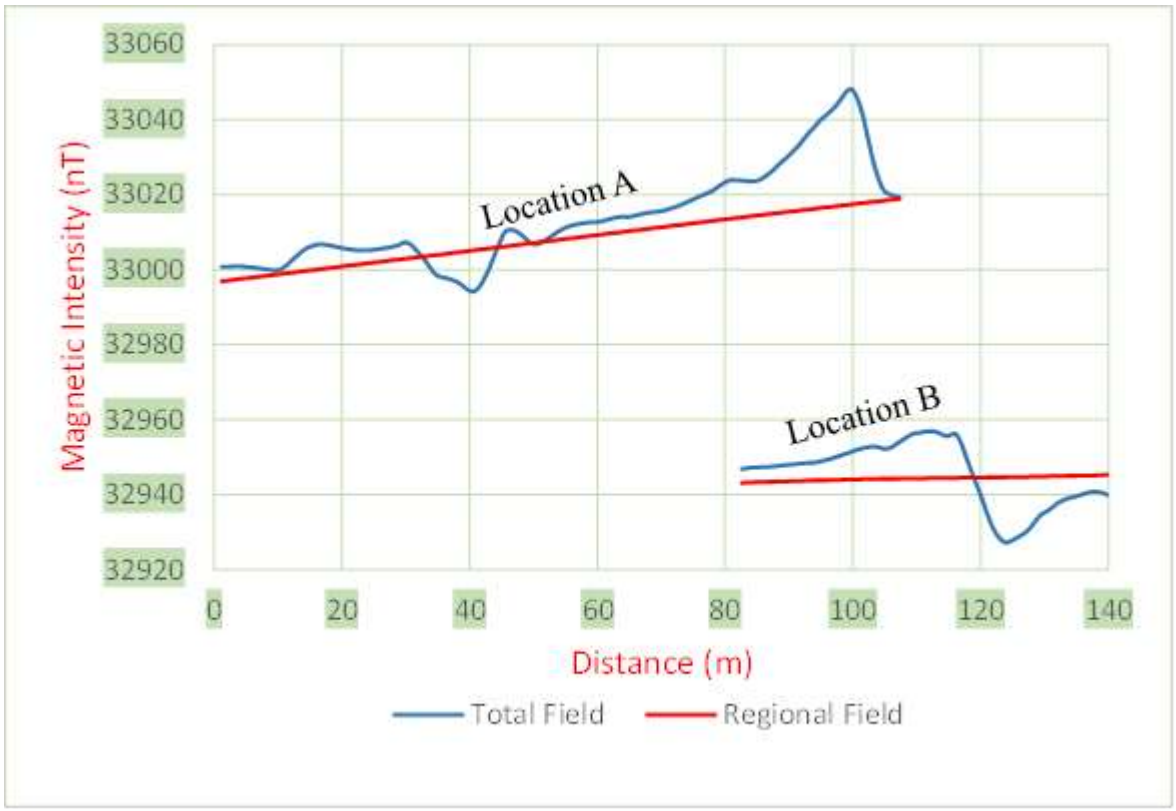

Figure 27. Total and Regional Magnetic Intensity Curves of Profile A and B. Magnetic intensity is greater at location A than B

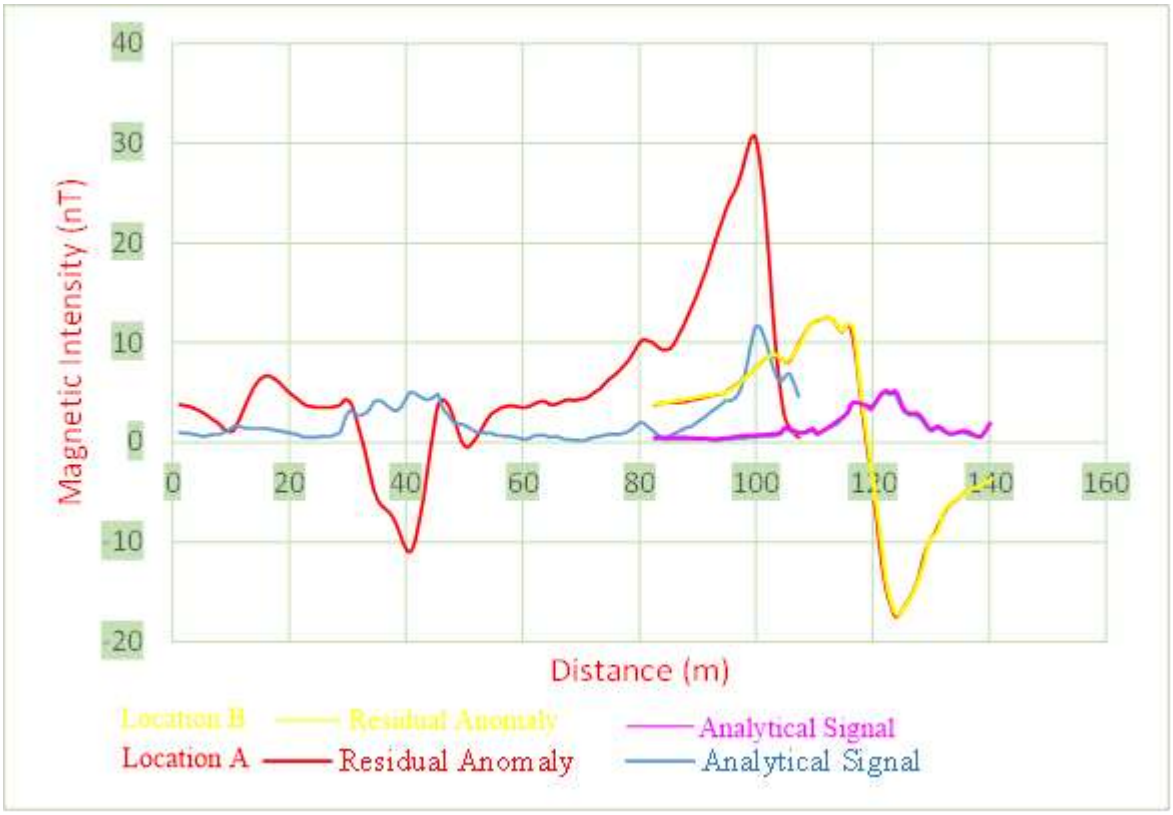

Figure 28. Residual Anomaly and Analytical Signal Profiles at Location A and B

Volume 66 (2020), No. 1
p. 1–32, ISSN 1802-5420
DOI 10.35180/gse-2020-0027

14 MAGNETIC ANOMALIES AND STRUCTURAL INTERPRETATION

Geomagnetic parameters for the potential field simulation of magnetic anomalies at both locations are presented in Table 1. Parameters are insignificantly higher at location B due to its geographic positioning at a relatively higher latitude. Amidst the three alternatives available for the description of the geomagnetic field vector, the total field strength (F) and the two magnetic directions (i.e. inclination (I) and declination (D)) concept was adopted. F = 33032nT and 33033nT; I = -12.734^{O} and -12.729, and D = -1.916^{O} and -1.912^{O} at location A and B. Descriptions typically exemplify the modelling of magnetic anomalies occurring at a very low geomagnetic latitude.

Table 1. Geomagnetic parameters of Location A and B

LOCATION	D (^{O})	I (^{O})	H (nT)	Z (nT)	F(nT)	X(nT)	Y(nT)
A	-1.916	-12.734	32219	-7281	33032	32201	-1077
B	-1.912	-12.729	32221	-7278	33033	32203	-1073

Notes: ***D - Magnetic declination; I - Magnetic Inclination; H - Horizontal Intensity of Magnetic Field Vector; Z – Vertical Component of Magnetic Field Vector; F - Total Intensity of Magnetic Field Vector; X – Northern Component of Magnetic Field; Eastern Component of Magnetic Field.***

Model parameters simulating the magnetic effect of the anomaly (Figures 29) at location A considers a 106 m long, nearly vertical magnetic source (fracture) dipping 80^{O} from the horizontal, with a susceptibility of 0.01, density of 2.0 gcm^{-3}, body width of 5 m, vertical extent of 20 m; occurring at a very shallow depth of 5 m below the surface to its top. Parameters modelling the observed magnitude of magnetic anomalies at location B (Figures 30) include a susceptibility of 0.01, density of 2.0 gcm^{-3}, width of 3 m, vertical extent of 12 m and a dip of 75^{O}; depth to the top of the anomaly is 5 m. Strike of the anomalies at both locations extends to infinity.

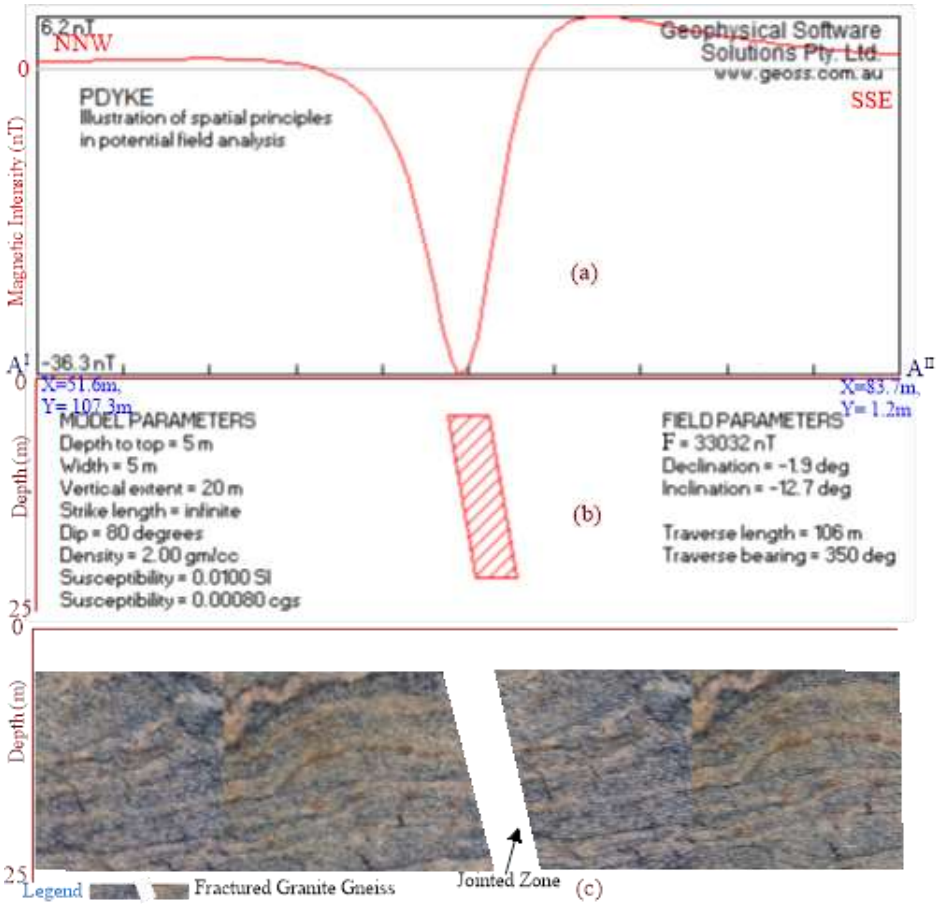

Figure 29. Geomagnetic Section along Profile A^{I} - A^{II}. Field and model parameters simulating the effect of the anomaly are also depicted. Magnetic anomaly is negative, and a simple geological interpretation ascribed the anomaly to the presence of long narrow fractures with an impressive vertical extent

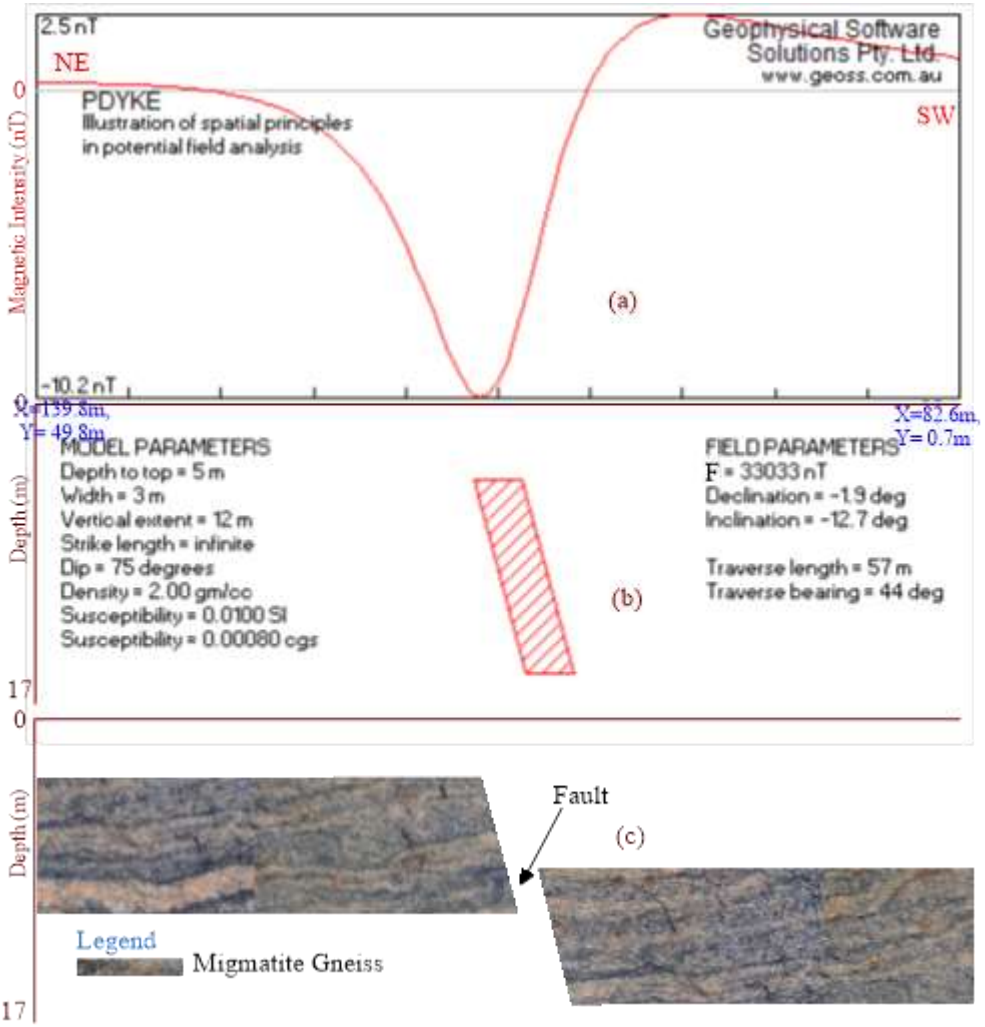

Figure 30. Geomagnetic Section along Profile B^{I} - B^{II} over a localized fault zone. Field and modelled parameters characterizing the magnetic anomaly are similarly shown in the figure. Anomaly is a normal fault with an estimated of 4.5 m

15 STRESS AND STRAIN DISTRIBUTION

Orientation of fractures (strain) is an important clue for the comprehension of the stress exertion on rocks. From the observed strain pattern, a pool of information can be obtained about the paleo-forces that operated within the area. Azimuths of delineated fractures are multidirectional, which in accordance to the frequency of occurrence are: NW – SE , NNW – SSE, and NE-SW (Figure 31).The perpendicular stress impress can be inferred to have been directionally exerted in the NE – SW, NNE –SSW, NW-SE.

Volume 66 (2020), No. 1
p. 1–32, ISSN 1802-5420
DOI 10.35180/gse-2020-0027

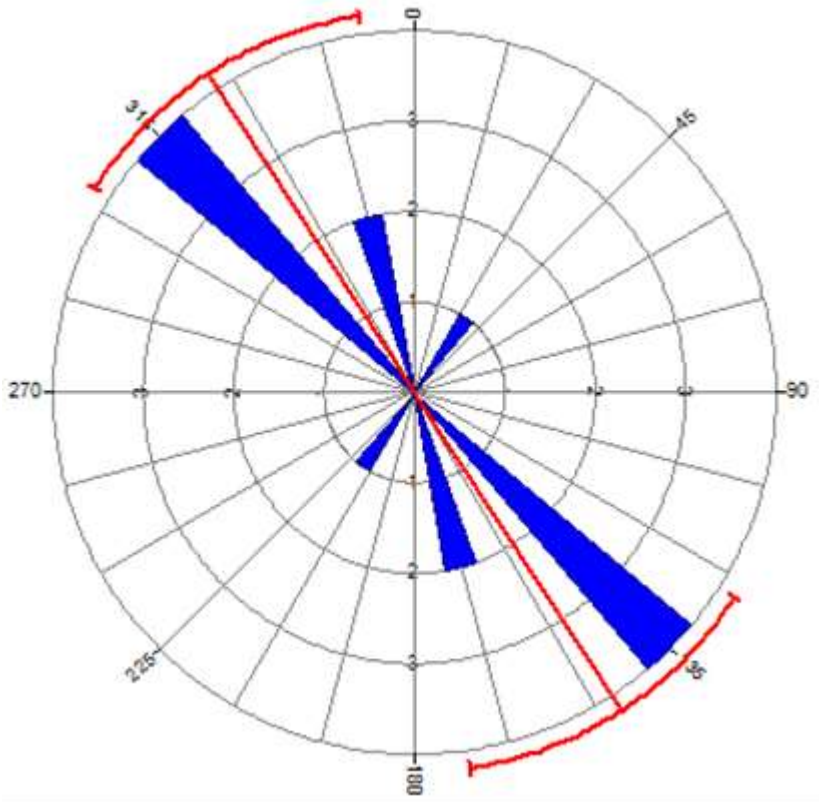

Figure 31. Rose Diagram Plot of Fracture Orientation in the Study Area

16 CONCLUSION AND RECOMMENDATIONS

Key deductions from the magnetic map interpretations include the presence of shallowly buried magnetic sources inferred as gneisses, and upon which the imprints of deformative forces are apparent; the predominance of NW – SE trending structurally induced magnetic anomalies, affirming the occurrence of geological fractures formed in response to Liberian orogenic stress exertion; consistent alignment of fractures with foliation fabrics of magnetic blocks (gneisses), and the interpretation of the subtle topographic scarp as an indicator or faulting activities in the area. The significance of this area as a prospective hydrogeological centre, and as an undesirable spot for high-rise building has been accurately evaluated from this study. The use of integrated geophysical approach, complemented by detailed geological studies may furnish greater information about the subsurface structural architecture.

REFERENCES

[1] AYAZ, M. D. and S. LASITHA. Application of Geophysical ground magnetic method for the Delineation of Geological structures. A study in parts of Villupuram District, Tamilnadu. *Journal of Geology and Geophysics*. 2015, 4:3, pp. 1-4.

[2] MIDDLETON, M., T. SCHNUR, P. SORJONEN-WARD and E. HYVONEN. Geologic Lineament Interpretation using the object based analysis approach: results of semi-automated analyses versus visual interpretation. *Geological survey of Finland*. 2015, Special paper 57, pp. 135-154.

[3] PAGEL, M. and J. L. LEROY (EDS). Source, transport and deposition of metals. Chapter 5. Structural environment. Rotterdam, Netherlands: A.A. Balkema, 1991.

[4] GUBBINS, D. and E. HERRERO-BERVERA. *Encyclopedia of geomagnetism and paleomagnetism*. Dordrecht: Springer, 2007.

[5] BURKE, K.C. and J.F. DEWEY. Orogeny in Africa. In: DESSAUVAGIE, T. F. J. and A. J. WHITEMAN (eds), Africa geology. University of Ibadan Press, Ibadan. 1972. pp. 583-608.

[6] DADA, S.S. Proterozoic evolution of Nigeria. In: OSHI (ed.) The basement complex of Nigeria and its mineral resources (A Tribute to Prof. M. A. O. RAHAMAN). Akin Jinad & Co. Ibadan. 2006. pp. 29-44.

Volume 66 (2020), No. 1
p. 1–32, ISSN 1802-5420
DOI 10.35180/gse-2020-0027

[7] GANDU, A.H, S.B. OJO and D.E. AJAKAIYE. A gravity study of the Precambrian rocks in the Malumfashi area of Kaduna State, Nigeria. *Tectonophysics*. 1986, 126, pp. 181-194.
[8] OLAYINKA, A.I. Geophysical siting of boreholes in crystalline basement areas of Africa. *J AfrEarth Sci*. 1992, 14, pp. 197-207.
[9] ABAA, S.I. The structure and petrography of alkaline rocks of the Mada Younger Granite Complex, Nigeria. *J. Afr Earth Science*. 1983, 3, pp. 107-113.
[10] ROEST, W.R., J. VERHOEF and M. PILKINGTON. Magnetic interpretation using the 3D analytic signal. *Geophysics.* 1992, 57(1), pp. 116-125.
[11] MACLEOD, I.N., K. JONES and T.F. DAI. 3D analytic signal in the interpretation of total magnetic field data at low magnetic latitudes. *Explor Geophys*. 1993, 24, pp. 679-688.
[12] MACLEOD, I.N., S. VIERRA and A.C. CHAVES. Analytic signal and reduction-to-the-pole in the interpretation of the total magnetic field data at low magnetic latitudes. In: *Proceedings of the third international congress of the Brazilian society of geophysicists*. 1993.
[13] PARLOWSKI, J., R. LEWIS, T.D. DOBUSH and N. VALLEAU. An integrated approach for measuring and processing geophysical data for the detection of Unexploded Ordnance. In: *Proceedings of symposium on the application of geophysics to engineering and environmental problems* (SAGEEP 1995), 1995, pp. 965-974.
[14] SMITH, M. J. and C.D. CLARK. Methods for the visualization of digital elevation models for landform mapping. *Earth Surface Processes and Landforms*. 2005, 30, pp. 885-900.
[15] MILLER, H. and V. SINGH. Potential field tilt—a new concept for location of potential field sources. *Journal of Applied Geophysics*. 1994, 32, pp. 213-217.
[16] ORUC, B. and H. SELIM. Interpretation of magnetic data in the Sinop area of Mid Black Sea, Turkey, using tilt derivative, Euler deconvolution, and discrete wavelet transform. *Journal of Applied Geophysics*. 2011, 74, pp. 194-204.
[17] SPECTOR, A. and F.S. GRANT. Statistical model for Interpreting aeromagnetic data. *Geophysics*. 1970, 35, pp. 293-302.
[18] REID, A.B., J.M. ALLSOP, H. GRANSER, A. J. MILLETT and I. W. SOMERTON. Magnetic interpretation in three dimensions using Euler deconvolution. *Geophysics.* 1990, 55, pp. 80-91.

Volume 66 (2020), No. 1
p. 1–32, ISSN 1802-5420
DOI 10.35180/gse-2020-0027